Lab on a Chip

RSC Publishing

CRITICAL REVIEW

View Article Online
View Journal | View Issue

Recent advances in microfluidic techniques for single-cell biophysical characterization

Cite this: *Lab Chip*, 2013, **13**, 2464

Yi Zheng,[ab] John Nguyen,[a] Yuan Wei[a] and Yu Sun*[abc]

Received 18th March 2013,
Accepted 16th April 2013

DOI: 10.1039/c3lc50355k

www.rsc.org/loc

Biophysical (mechanical and electrical) properties of living cells have been proven to play important roles in the regulation of various biological activities at the molecular and cellular level, and can serve as promising label-free markers of cells' physiological states. In the past two decades, a number of research tools have been developed for understanding the association between the biophysical property changes of biological cells and human diseases; however, technical challenges of realizing high-throughput, robust and easy-to-perform measurements on single-cell biophysical properties have yet to be solved. In this paper, we review emerging tools enabled by microfluidic technologies for single-cell biophysical characterization. Different techniques are compared. The technical details, advantages, and limitations of various microfluidic devices are discussed.

Introduction

The cell, the basic functional unit of living organisms, maintains and senses the physiological environment within the organism both chemically and physically.[1–4] The unique biochemical and biophysical properties enable a cell to fulfill its specific functions and adapt to its surrounding environment. Physiological changes within the cells are accompanied by chemical and physical modifications and reorganization. Thus, pathological cells can be identified biochemically and/or biophysically. Biochemical properties of pathological cells have been under intensive study, and many biochemical markers have been developed to identify target cells out of a heterogeneous population.[5,6] The biophysical properties of cells also play important roles in various biological processes and are involved in the regulation of gene expression, differentiation, migration, and metabolic activities.[2,7] However, although research on the physical properties of cells has provided strong evidence about the capability of physical properties as potential markers for identifying cell types, most biophysics research was limited to proof-of-concept demonstrations. The lack of clinical relevance is due to the very low measurement throughput and tedious operation procedures of conventional techniques for measuring the biophysical properties of cells.[4,7–9] Compared to conventional techniques, the advantages of small sample volume, integration capability, biocompatibility and fast response make microfluidic technologies attractive for studying cells. Recent decades have witnessed significant advances of microfluidic technologies for biochemical characterization of cells.[10,11] Microfluidics is extending its way into the characterization of single-cell biophysical properties.[12–14]

In this review, we summarize existing microfluidic technologies for characterizing biophysical properties of individual cells (*i.e.*, mechanical and electrical properties). Within each section, we first provide an introduction of a technique. We then classify various techniques based on their working mechanisms and discuss their advantages and limitations. Finally, we present perspectives on the challenges for diagnostic applications and future directions of microfluidic technologies for single-cell biophysical characterization. This review is focused on discussing techniques for characterizing single-cell mechanical and electrical properties. Microfluidic techniques for studying the roles of mechanical and electrical stimuli in the regulation of differentiation, migration, and metabolic activities have been reviewed elsewhere.[3,4,13]

Mechanical characterization techniques

The association between cell deformability and human diseases has been of interest since the 1960s.[15,16] The deformability of nucleated cells is determined by the membrane, the cytoskeletal network (actin filaments, intermediate filaments, and microtubules), and its interaction with the nucleus, while the deformability of red blood cells (RBCs) is determined by the membrane skeleton network and the interaction between the membrane skeleton and membrane integral proteins.[4,17,18] Physiological and pathological changes

[a]*Department of Mechanical and Industrial Engineering, University of Toronto, Toronto, ON, Canada. E-mail: sun@mie.utoronto.ca; Fax: 1-416-978-7753; Tel: 1-416-946-0549*
[b]*Institute of Biomaterials and Biomedical Engineering, University of Toronto, Toronto, ON, Canada*
[c]*Department of Electrical and Computer Engineering, University of Toronto, Toronto, ON, Canada*

Table 1 RBC deformability decrease under pathological conditions

Disease	Possible genetic and molecular cause	Reference
Malaria	Interruption of cytoskeleton network by parasite protein	17, 22–25
Hereditary spherocytosis	Low cytoskeleton density	17, 26–28
Sickle cell disease	Polymerized and deoxygenated hemoglobin	29, 30
Sepsis	Altered spectrin interaction	31–33
Diabetes	Not clear	34–36
Stored RBCs	Depletion of ATP and Nitric oxide	37, 38

can alter the cytoskeleton composition, reorganize the network structure, and change the protein density. As a result, cell deformability can be used as an intrinsic marker for identifying pathological conditions.[8,19,20] For example, deformability is known to play a crucial role in the mobility of cancerous cells;[4,21] and a decrease in RBC deformability has been proven to be relevant in several human diseases (see Table 1).

Compared to existing experimental tools, such as atomic force microscopy, micropipette aspiration, optical tweezers, and magnetic tweezers, which are all difficult to use and have a low testing speed, microfluidics offers the potential for high-throughput mechanical measurement of single cells.[4,10,12,13] For characterizing the mechanical properties of a cell, the cell must be deformed. Thus, we classify microfluidic technologies for cell deformability measurements according to the mechanical stimuli used to deform the cell. Table 2 summarizes these techniques and their working mechanisms, cell samples, key technologies and observations, and reported throughput. For those where throughput was not reported, the total number of tested cells is listed in Table 2 in order to provide a sense of the devices' throughput.

Structure-induced deformation (constriction channels)

Constriction channels, which are marginally smaller than the diameters of tested cells, provide an efficient method to generate mechanical stimuli. Cells driven through a constriction channel are squeezed by the walls of the constriction channel. Multiple parameters, such as transit time, elongation and recovery time, in association with cell deformability can be quantified. Moreover, constriction channels can be easily fabricated with standard microfabrication techniques and are able to provide an environment to mimic *in vivo* capillaries. With the use of high-speed imaging or electrical impedance measurements, constriction-channel devices are capable of achieving a higher throughput than most other deformability measurement approaches. Due to these merits, constriction channels have been used to measure the deformability of RBCs,[22,23,39–44] leukocytes[45] and cancer cells.[46,47]

Due to the human capillary-like environment and the physiological relevance of RBC deformability, RBCs are mostly studied in the majority of existing constriction channel-based devices. The first demonstration of microfluidic constriction channels for RBC deformability characterization was reported in 2003.[22] In this study, constriction channels with various diameters were used to study the deformability changes between healthy RBCs and malaria parasite-infected RBCs at different stages (early ring stage, early trophozoite, late trophozoite, and schizont). They found that the deformability of malaria-infected RBCs decreases as the parasite progresses from the early ring stage to a schizont, while healthy RBCs are exceptionally deformable and are even able to travel through the constriction channels blocked by infected RBCs. In addition to RBC deformability, white blood cell (WBC) deformability was also studied using microfluidic constriction channels. Rosenbluth *et al.* demonstrated the clinical relevance of their microfluidic constriction channel device in sepsis and leukostasis.[45] The reported device consists of a network of 64 constriction channels. High-speed imaging was used for measuring cell transit time. They used patient samples to show that cell transit time increased for diseased samples compared to control samples (Fig. 1(a)). In another study, breast cancer cell lines (MCF-7 and MCF-10A) were flown through a constriction channel to distinguish non-malignant and malignant cells.[46] According to the reported results, transit velocity is not significantly affected by cell types, and the transit time difference is mainly determined by the entry time. Different cell types can be distinguished on the basis of scatter plots of cell volume and entry time.

Besides imaging, microfluidic constriction channels can also be used together with other measurement techniques to achieve multiple parameter measurements for cell type classification. We recently developed a microfluidic device (Fig. 1(b)), which combines a constriction channel and impedance measurements.[39] Detection involves only electrical signals; hence, it enables a throughput higher than 100 cells s^{-1}. The multiple parameters quantified as mechanical and electrical signatures include transit time, impedance amplitude ratio, and impedance phase increase. Histograms compiled from 84 073 adult RBCs and 82 253 neonatal RBCs reveal different biophysical properties across samples and between the adult and neonatal RBC populations. Bow *et al.* demonstrated a deformability-based RBC testing device combining constriction channels and fluorescence measurement. They showed a population-based correlation between biochemical properties, such as cell surface markers, and mechanical deformability.[23] They also showed experimentally that the entrance geometry of the constriction channel has a significant impact on RBC transit time, and developed a dissipative particle dynamics model to interpret the parasitic effect on RBC deformability. An optical stretcher was also introduced to enhance the sensitivity and reliability of a constriction channel-based microfluidic device.[40] Scatter plots

Table 2 Microfluidic devices for single-cell mechanical characterization

	Techniques	Targeted cells	Summary	Throughput[a]	Ref.
Structure-induced	Constriction channels of different cross-sectional areas	Malaria infected RBCs	Uninfected RBCs can readily travel through the constriction channel. RBCs become less deformable as the stage of malaria infection progresses.	N/A	22
	Cuneiform constriction channel array + fluorescence	Malaria infected RBCs	Entrance geometry of the constriction channel has a significant impact on RBC transit time. Deformability measurements of ring stage *P. falciparum*-infected and uninfected RBCs show significant overlap.	$\sim$100 cells min^{-1}	23
	Constriction channel + impedance measurement	Adult and neonatal RBCs	Characterization of multiple parameters (transit time, impedance amplitude and impedance phase) improves the classification accuracy.	100–150 cells s^{-1}	39
	Constriction channel + optical pressure	RBCs from healthy donors and leukemia patients	Recovery time of RBCs from healthy donors and leukemia patients was found to be significantly different.	N = 140	40
	Constriction channel array	Blood cells from AML and ALL patients, and HL-60 cell lines.	Transit time of WBCs from AML patients with leukostasis symptoms is significantly higher than the WBCs from AML patients without leukostasis symptoms and ALL patients.	50–100 cells min^{-1}	45
	Constriction channel	MCF-7 and MCF-10A	The different transit time is mainly contributed by the longer entry time of MCF-7.	$N \approx 100$	46
	Constriction channel + impedance measurement	MC-3T3 and MLO-Y4; EMT6 and EMT6/AR1.0	Cells with comparable sizes (EMT6 and EMT6/AR1.0) were classified based on their different deformability and electrical properties.	$\sim$1 cells s^{-1}	47
	Constriction channel + volume measurement	HeLa	Controlled Hela cells have longer transit time than Hela cells treated with latrunculin A and cytochalasin B.	800 cells min^{-1}	48
	Constriction channel + deformable membrane	MCF-7 and MCF-10A	MCF-7 and MCF-10A can be distinguished on the basis of transit time.	N = 150–200	49
Fluid-induced	Inertial focusing + hydrodynamic stretching	Leukocytes and malignant cells in pleural effusions; pluripotent stem cells	The prediction of disease states in patients with cancer and immune activation achieved a sensitivity of 91% and a specificity of 86%.	$\sim$2000 cells s^{-1}	19
	Straight microchannel	RBCs and fixed RBCs	Effects of diamide and glutaraldehyde on RBC dynamics were examined by visual observation of cells when flowing through a microchannel.	N/A	50
	Hyperbolic converging microchannel	RBCs	The results prove that hyperbolic shape is more efficient in deforming RBCs.	N/A	51
	Shear stress + resistance measuring	RBCs and fixed RBCs	The resistance signal generated by integrated electrodes is correlated to the deformation of RBCs.	N = 72	83
Electroporation-induced	Microfluidic channel + high electrical field	MCF-10A and MCF-7	More malignant and metastatic cell types exhibit more significant swelling.	5 cells s^{-1}	61
	Microfluidic channel + high electrical field	Controlled mouse RBCs, mouse RBCs with deficiencies of ankyrin, β-adducin and Tmod1	Time taken for complete electroporation-induced lysis can be correlated to the defects in the cytoskeleton network.	2000–3000 cells/sample	63
Optical stretcher	Microfluidic channel + laser beam	RBCs; BALB 3T3	Optical deformability can be used to differentiate cells by measuring the differences in elastic response.	N/A	67
	Microfluidic channel + laser beam	MCF-10A, MCF-7 and modMCF-7; MDA-MB-231; BALB/3T3 and SV-T2	Cancer cell lines are significantly more deformable than normal cells.	N/A	70
	Microfluidic channel + laser beam + microcouplers	RBCs	A two-axis active microcoupler capable of generating substantial displacement for accurate alignment of buried optical fibers was developed.	N/A	71

Table 2 (*Continued*)

	Techniques	Targeted cells	Summary	Throughput[a]	Ref.
	Microfluidic channel + laser beam	Healthy and cancerous oral squamous cells	Cancer cells showed a higher mean deformability and increased variance.	N = 200–300	74
DEP-induced	Microfabricated electrodes	CHO-K1 and U937	Cell deformation was interpreted into mechanical properties using an analytical model.	N = 15	77
	Microfabricated electrodes	SiHa and ME180	A FEM model was developed to extract the Young's modulus of cells.	N = 14	78
	ITO electrodes + microchamber array	Healthy and spherocytosis RBCs	RBCs from patients with spherocytosis are less deformable than RBCs of healthy volunteers.	N = 200–300 for each cell type	79
Aspiration-induced	Funnel chain + pressure attenuator	Healthy and malaria RBCs	Malaria infected RBCs were proven less deformable than normal RBCs.	N = ~100 for each cell type	81
	Microfluidic pipette + impedance measurement	MC-3T3	MC-3T3 was characterized by impedance spectroscopy and micropipette aspiration.	N = 18	82

[a] Throughput: For those references that explicitly reported speed/throughput, speed/throughput is listed directly in the table. For those references where speed/throughput was not explicitly reported, we calculated speed/throughput using the data plots (*e.g.*, histograms) presented in those references

compiled from transit time, elongation, and recovery time measured by this device proved effective for the discrimination of RBCs from normal donors and leukemia patients.

Other applications of microfluidic constriction channels include the use of wedge-shaped constriction channels to measure the surface area and volume of a large population of RBCs,[41–43] and a microfluidic manometer to measure the pressure drop due to the presence of a cell in the constriction region, which correlates with the stiffness of the cell, by observing the displacement of the downstream fluid–fluid interface.[44] Despite the advantages of the constriction channel technique, cell volume and adhesion between the cell membrane and channel walls are coupled with cell deformability. Consequently, a longer transit time does not necessarily mean lower deformability since larger and stickier cells can also lead to a longer transit time. Efforts have been made to take the cell volume/size effect into account. For example, Adamo *et al.* reported a microfluidic device for probing both cell volume and transit time. Comparisons of cell transit time were made among cells with a similar volume[48]. They demonstrated that Hela cells in the control group have a longer transit time than Hela cells treated with latrunculin A and cytochalasin B. The size of the constriction channel can also be adjusted on demand according to targeted cell size (MCF-7 and MCF-10A).[49] However, there exists no technique that is capable of characterizing the adhesion (or friction) between the cell membrane and channel walls. In addition, since the diameter of the constriction channel is smaller than the diameter of the targeted cells, the channel is susceptible to clogging. Using an array of constriction channels appears to be a potential solution to the clogging issue.

Fluid-induced deformation

RBCs are highly deformable and can easily deform under fluid shear stress inside blood vessels. Having micrometer dimensions, which are comparable with *in vivo* capillaries, microfluidic channels provide an ideal tool for investigating RBC deformability. Compared to constriction channels, the microfluidic channels used to generate shear stress are larger than RBCs. Thus, RBCs are deformed by fluid shear stress instead of the channel's confinement structures. The deformation index (DI) or stretch ratio quantified *via* high-speed imaging has been used as a measure of RBC deformability.[36,50,51] Forsyth *et al.* studied the deformability and dynamic behavior of chemically ''stiffened'' RBCs using a simple straight microfluidic channel, revealing three different types of motion due to the increased shear rate in the microfluidic channel: stretching, tumbling, and recoiling.[50] Besides straight channels, a hyperbolic converging microchannel was also developed for assessing RBC deformability by measuring extensional flow-induced deformation.[51] The results confirmed that extensional flow is more efficient in causing RBC deformation. Shear stress generated in microfluidic channels was also used to measure the dynamics of shear-induced adenosine triphosphate (ATP) release from RBCs. In ref. 52, RBCs were driven through a microfluidic channel with a cross-sectional area of 20 × 20 μm, while the amount of ATP released was measured by counting the photons emitted from a standard luciferase-ATP bioluminescent reaction. Cell deformation and dynamics were quantified simultaneously using high-speed imaging.

Although shear stress proves effective for investigating RBC deformability, the low magnitude of shear stress is typically not able to deform other types of cells. Gossett *et al.* recently reported a hydrodynamic-stretching microfluidic device for identifying malignant cells in a human pleural fluid sample with a measurement speed of ~2000 cells s^{-1} (see Fig. 1(c)).[19] Cells are focused towards a narrow streamline near the center of the microfluidic channel and delivered to a junction of two orthogonal channels at a high flow rate, where the cells undergo mechanical stretching. Meanwhile, cell deformations are captured using a high-speed camera and images are then analyzed to extract the cell volume and deformation index (DI). The results revealed that cancerous cells in pleural fluid have

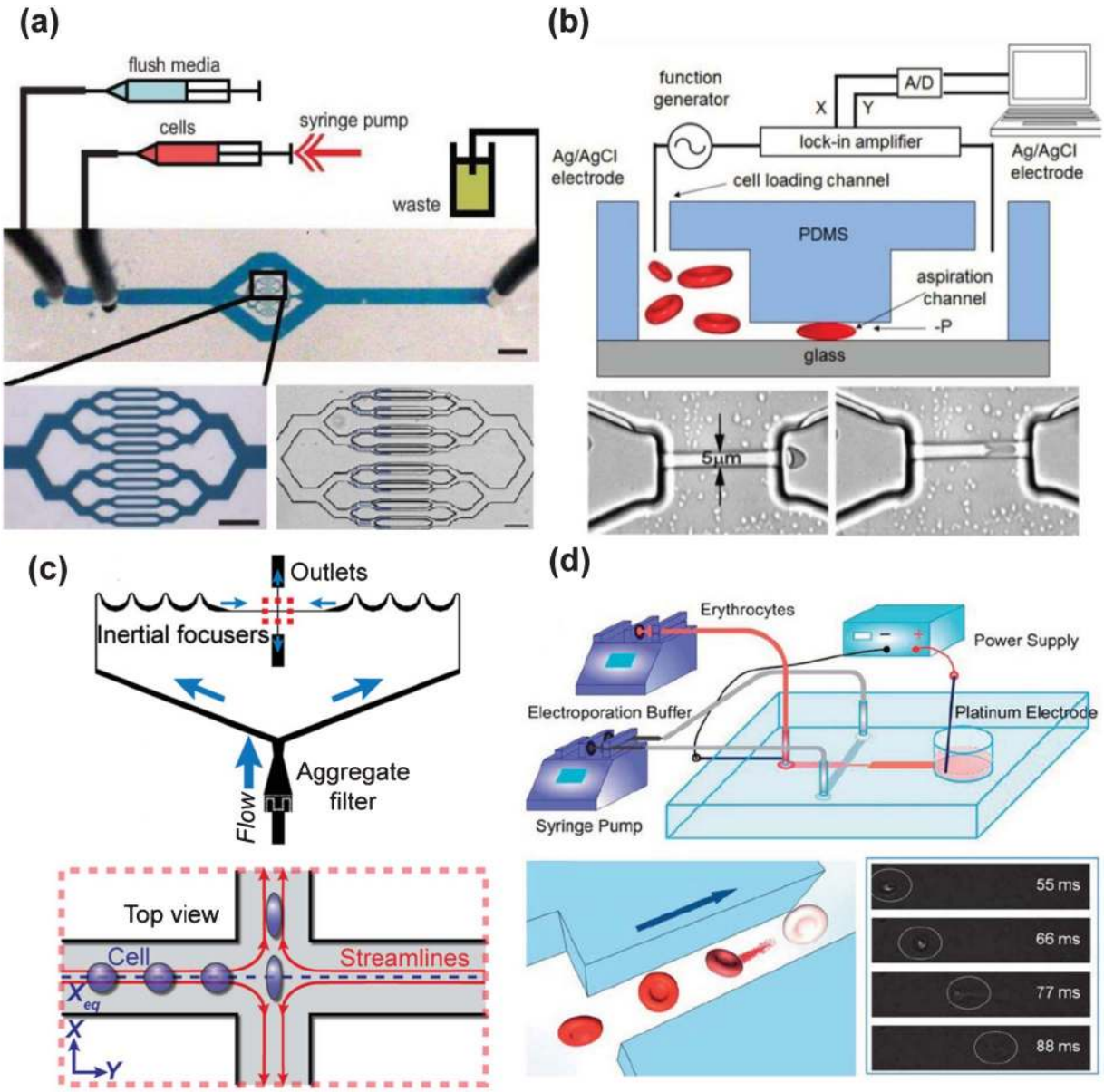

Fig. 1 (a) A network of bifurcating microfluidic channels for blood cell deformability measurement. The transit time of the individual cells are measured using a high-speed camera. Reproduced with permission from ref. 45. (b) A microfluidic system for electrical and mechanical characterization of RBCs at a speed of 100–150 cells s^{-1}. The transit time is obtained from electrical impedance data captured during RBCs flowing through the constriction channel. Reproduced with permission from ref. 39. (c) Hydrodynamic stretching microfluidic device. Cells are focused to the center lines of the channels by inertial force and stretched by fluid pressure. Cell deformation is measured by analyzing images recorded by a high-speed camera. Reproduced with permission from ref. 19. (d) Electroporation-induced RBC lysis. Time-lapse images of RBCs are recorded by a high-speed camera as the cells flow through the channel, while a constant DC voltage is applied. Cell lysis time is correlated with RBC deformability. Reproduced with permission from ref. 63.

larger volumes and are more deformable (higher DI values) than benign cells. This approach achieved both a high testing speed and larger deformation of tested cells. The authors predicted disease states in patients with cancer and immune activation with a sensitivity of 91% and a specificity of 86%.

In fluid-induced deformation-based microfluidic devices, channel dimensions are larger than cell diameters. DI is used as the deformability indicator and is not affected by the adhesion between cell membrane and channel walls (*vs.* constriction channel). However, since cells of different sizes may experience different forces due to non-uniformity in the shear stress and hydrodynamic pressure within the microchannel, DI is still associated with cell volume. More specifically, shear stress is highest near channel walls and is almost zero in the center of the channel. As a result, RBCs with larger volumes experience higher shear stress on the edges causing larger deformation compared to cells with smaller volumes. Within the hydrodynamic-stretching microfluidic device, the highest compressive pressure appears at the center of the junction where the cells are stretched, which causes

cells with different volumes or shapes to be exposed under a different pressure environment. To address this issue, cell volume is measured as an independent parameter and used as a reference for cell-type classification.[19]

A limitation of fluid-induced deformation-based microfluidic devices is the use of high-speed imaging (tens of kHz) for measuring DI. High-speed cameras are often costly and must be used on a microscope, making the overall microfluidic system bulky. Furthermore, since real-time image data transfer from a high-speed camera to the computer hard drive is technically difficult to achieve, images are stored in the camera's on-board memory for later off-line transfer. Since state-of-the-art high-speed cameras typically have only a few GB of on-board memory, after recording for a few seconds, the experiment must be stopped for image data transfer. Processing massive amounts of image data also costs tremendous computational effort and time. Advances in high-speed cameras and hardware-based image processing techniques, such as FPGA-based techniques, will possibly be able to solve the data transfer problem. Additionally, opto-microfluidics, microfluidic devices integrated with optical components, also seems a promising way to tackle this problem. Integrating on-chip lenses and CMOS chips[53–56] can achieve real-time performance and in the meantime, eliminate the need for the use of bulky microscopes.

Electroporation-induced deformation

Electroporation is a technique used for introducing foreign molecules, such as DNA and proteins, into cells. The concept of electroporation capitalizes on the relatively weak nature of the phospholipid bilayer's hydrophobic/hydrophilic interactions and its ability to spontaneously reassemble after a disturbance.[57] Thus, a voltage shock can disrupt areas of the membrane temporarily, allowing polar molecules to pass. The membrane then can re-seal and leave the cell intact.[57–59] Swelling or expansion in cell size accompanies the cell's electrical property changes,[60] which is caused by the influx of molecules through the open pores in the cell membrane (*vs.* dielectric force in DEP-induced deformation). Recently, a few studies correlated electroporation-induced cell deformation and lysis to cell deformability changes. Bao *et al.*[61] developed microfluidic electroporative flow cytometry to study the deformability of single cells. A constant DC voltage was established across the microchannel, which concentrated the electric field to yield repeatable cell exposure to uniform electrical fields. When cells were flown through the microchannel, the swelling of cells was recorded by imaging and quantified as a deformability indicator. Deformability changes of breast cancer cell lines[61] and the expansion of the nuclei of circulating tumor cells (CTCs) were tested using the system.[62] The capability to detect RBCs with deficiencies of the cytoskeletal protein network was also demonstrated (see Fig. 1(d)).[63] The achieved throughput was about 5 cells s^{-1}.

It is notable that electroporation efficiency is also dependent on cell volume. Under the same uniform electrical field, the effective voltage across the cell membrane is a function of cell diameter.[64] Hence, cells with larger diameters are exposed to higher voltages and are more easily porated. In addition, the plasma membrane of different cell types (*e.g.*, metastatic tumor cells *vs.* non-metastatic tumor cells) can possess different poration properties. In other words, some cell types may be more susceptible to electrical fields than others. Thus, based on electroporation-induced expansion or swelling alone, it can be inaccurate to conclude that cell deformation is caused by cell deformability rather than the membrane's poration susceptibility to electrical voltages.

Optical stretcher

Optical trapping was discovered in 1970[65] when radiation pressure from laser light was found to be able to accelerate and trap micron-sized dielectric particles. Light interacts with a particle by imparting some of its momentum onto it, thus exerting a force on the particle. If the particle is not centered on the optical axis of the beam, a restoring force is exerted on the particle to keep it on the optical axis. Optical stretchers utilize two slightly divergent Gaussian beams to trap an object in the middle. This concept was used to deform and measure the stress profiles of erythrocytes, which led to the development of the first optical stretcher device reported in 2000.[66] The setup was then demonstrated to stretch BALB 3T3 fibroblasts and measure their viscoelastic properties.[67]

A typical optical stretcher system consists of a microchannel for loading cells into the testing region and two laser fibers located on the sides of the passageway (see Fig. 2(a)).[68] Cells flowing through the microfluidic channels are serially trapped and deformed with the two counter propagating divergent laser beams.[69,70] For trapping and stretching cells in the optical stretcher, the alignment of the fibers is crucial. In order to improve alignment, a platform capable of adjusting fiber positions was developed[71] using pneumatically driven manipulators. The femtosecond laser technique has been utilized for the fabrication of optical stretcher-based microfluidic devices.[72,73] By direct writing of both optical waveguides and microfluidic channels, the alignment problem can be mitigated significantly. The deformability of human cancer cell lines,[69,70] red blood cells[71] and patient oral squamous cells[74] was characterized using optical stretchers.

DEP-induced deformation

When polarized in an electric field, biological cells will experience a dielectric force, which is well known as a DEP force.[75,76] Electro-deformation devices utilize the DEP force for trapping and generating mechanical stimuli to quantify the deformability of individual cells.[77,78] The Young's modulus of tested cells can be extracted with either analytical models or numerical simulation. For improving the throughput of electro-deformation devices, a single-cell microchamber array device[79] was proposed. The device is able to trap individual RBCs in a large array of micro-wells integrated with DEP electrodes. ITO electrodes also allow the correlation of RBC deformation with cell surface and cytosolic characteristics (Fig. 2(b)). However, due to the time-consuming procedure of cell trapping, the overall throughput of this device is still rather limited. On the other hand, the complex physical phenomena involved in electro-deformation and unknown cell electrical properties pose difficulties in extracting forces experienced by an electro-deformed cell.[75,77,78] Since the DEP force is determined by the dielectrical properties of cells, DEP-

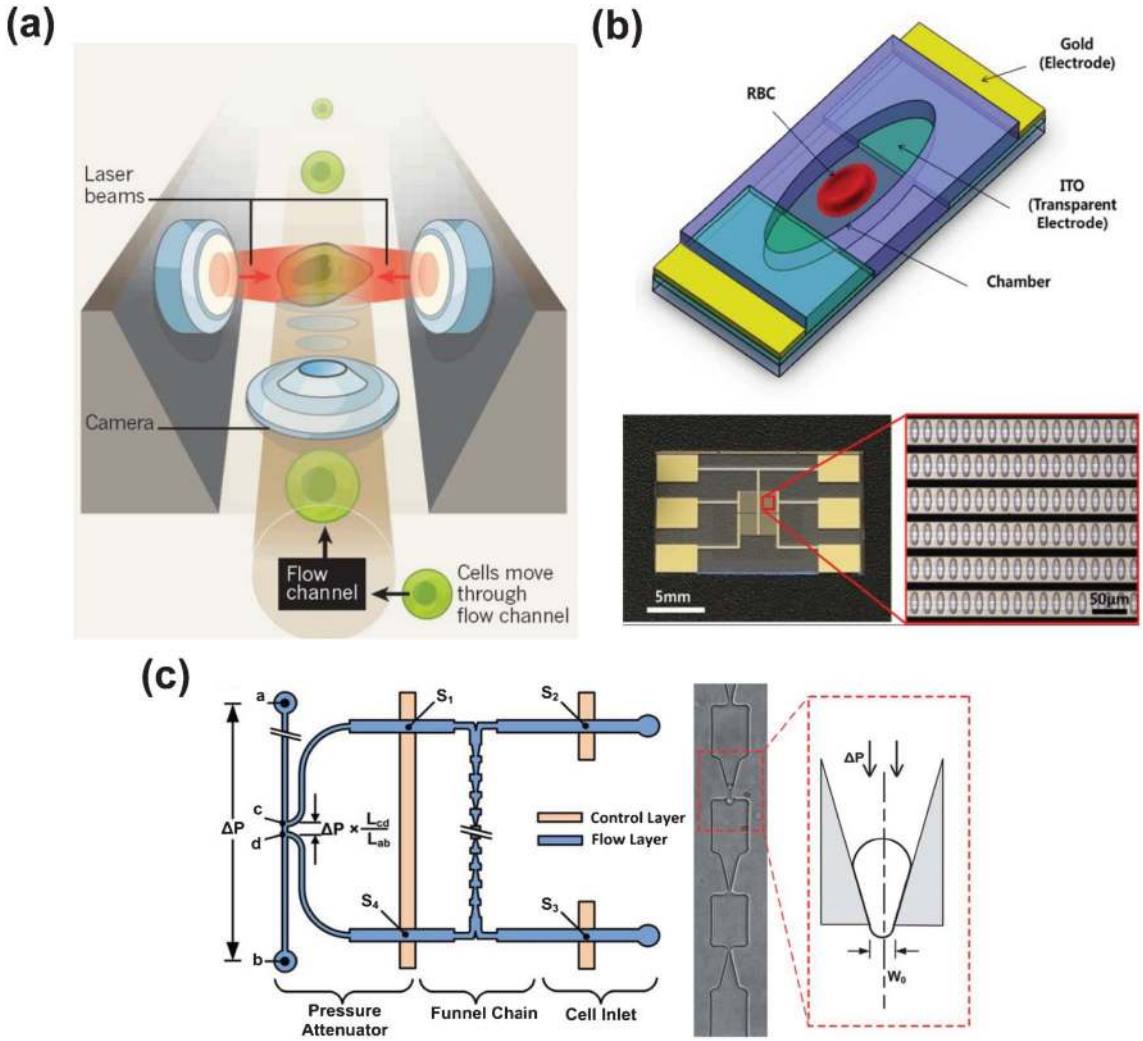

Fig. 2 (a) An optical stretcher. Cells travel along a flow channel integrated with two opposing laser beams. Cells are trapped and deformed optically, and cell deformation images are recorded. Reproduced with permission from ref. 68. (b) A single-cell microchamber array for electro-deformation. An array of microchambers integrated with DEP electrodes is used to trap individual RBCs and apply a DEP force. Reproduced with permission from ref. 79. (c) Microfluidic pipette aspiration of cells using a funnel channel chain. Reproduced with permission from ref. 81.

based techniques can also be used to electrically characterize cells, which is discussed in the electrorotation section under electrical characterization.

Aspiration-induced deformation

Pipette aspiration is a conventional technique for studying the mechanical properties of single cells.[80] The mathematical models in conventional pipette aspiration have been adopted in microfluidic characterization of cells. Fig. 2(c) shows a microfluidic pipette aspiration device.[81] Single cells are infused into a microfluidic channel and deformed through a series of funnel-shaped constrictions. Malaria-infected RBCs were tested using both membrane cortical tension and threshold pressure as readouts. We developed a microfluidic device for single-cell electrical and mechanical characterization using impedance spectroscopy and micropipette aspiration.[82] Cellular deformation was recorded as a function of increasing pressure, while cellular impedance was measured *via* two Ag/AgCl electrodes inserted into the culture medium. With pipette aspiration and equivalent circuit models, both mechanical properties and dielectric properties of single cells were quantified. In addition to throughput limitation, the rectangle-like cross-section in microfluidic pipette aspiration devices can cause concerns about the validity of applying conventional pipette aspiration models.

Electrical characterization techniques

Besides mechanical deformability, electrical properties of cells are also important physical properties, serving as the basis of counting, trapping, focusing, separating, and the characterization of single cells.[84,85] Early work on cell electrical measurements dates back to the 1910s,[86–88] when approximate hemoglobin conductivity inside RBCs was reported. The single shell model proposed by Pauly and Schwan in the 1950s laid

the foundation for interpreting the electrical properties of cells, where the cell is modeled as a spherical cytoplasm surrounded by a thin dielectric membrane.[89,90] Generally, the electrical properties of a plasma membrane are affected by the membrane morphology, lipid bilayer composition and thickness, and embedded proteins.[91–93] Electrical properties of the cytoplasm are influenced by the intracellular structures and physiological conditions (*e.g.*, nucleus-to-cytoplasm ratio and ion concentrations inside the cell).[94–96] Early techniques were only capable of measuring the average electrical properties of a cell population. The patch-clamp technique, developed in 1976 is capable of electrical characterization of single cells.[97] However, a patch-clamp typically takes tens of minutes to test one cell. Because of the capability of manipulating micro-scaled objects and integrating microelectrodes on-chip, microfluidic techniques have gained momentum in single-cell electrical characterization in recent years. Table 3 summaries and classifies microfluidic techniques for the electrical characterization of single cells.

Microfluidic Coulter counter

The Coulter counter monitors the DC resistance of a small orifice as microparticles pass through. Since the cell membrane acts as an insulating layer at DC, the presence of the cell alters the resistance of the orifice by replacing the conductive liquid. Well established models are available for correlating DC resistance changes to cell volumes. Several designs have recently been proposed to improve the microfluidic Coulter counter's performance. For instance, two-dimensional sheath flow focusing was demonstrated to overcome the clogging issue;[98] and throughput of microfluidic Coulter counters was improved using multiple-orifice designs.[99]

One challenge for microfluidic Coulter counters lies in the selection of the electrode material. Ag/AgCl non-polarizable electrodes, which work well in the conventional Coulter counter, are an ideal choice. Nonetheless, integrating Ag/AgCl electrodes into microfluidic channels is complex, and Ag/AgCl electrodes have a limited lifetime.[100,101] Although other metal electrodes can be more readily integrated into microfluidic channels, the electrical double layers formed between the interface of electrodes and the liquid, which are mainly capacitive, pose difficulties in applying DC signals. Methods for minimizing the electrical double layer effect include the modification of the electrode surface roughness in order to increase the surface area[102] and the utilization of polyelectrolytic salt bridges (PSBEs)[103] or polyelectrolyte gel electrodes (PGEs).[104] Most recently, a DC impedance-based microcytometer device integrating PGEs was reported for CTC cell detection. Sheath flow is used for focusing cells and preventing cell adhesion to chambers and channels (see Fig. 3(a)). CTCs were successfully detected in blood samples from breast cancer patients.[105] Besides the electrode design that demands special design consideration, the model used in the conventional Coulter counter to calculate particle volumes is not directly applicable to microfluidic Coulter counter devices, due to the different electrode configuration and channel geometry.[106,107] A microfluidic Coulter counter is limited to counting and sizing single cells, but incapable of characterizing their electrical properties.

Electrorotation

When a cell/particle is placed in a non-uniform electrical field, a force is exerted on the induced dipole and can cause the cell to either move (DEP) or rotate (ROT).[75,108] Maxwell's mixture theory is commonly used to interpret DEP and ROT data, for associating the complex permittivity of the suspension to the complex permittivity of the particle/cell.[75,108] The DEP force and ROT torque are proportional to the real and imaginary parts of the Clausius–Mossotti factor, respectively.[9] Although DEP and ROT are closely related, ROT is more suitable for single-cell electrical characterization since in ROT, the cells are only rotated at a certain position in the electric field. Thus, the amplitude of the electric field remains unchanged, which is suitable for fitting the rotation spectra to determine intrinsic electrical properties of single cells (*e.g.*, specific membrane capacitance, cytoplasm conductivity and cytoplasm permittivity). Differently, forces in DEP are determined by the electric field gradient. A constant electric field gradient is technically challenging to achieve. Furthermore, the rotation rate is only determined by the rotation force (constant as a cell rotates) and the viscosity of the suspension medium in ROT, which can be readily measured, whereas the DEP force (varying as a cell moves) is difficult to quantify. DEP was demonstrated to electrically characterize cells by curve fitting of the Clausius–Mossotti factor spectra or cell count spectra. However, since the spectra are not from the measurements of the same cells, only average electrical properties of a cell population can be obtained.[109–111] More details on DEP and ROT models can be found in other reviews.[9,112]

The most popular ROT setup uses four electrodes connected to sine waves in phase quadrature.[91,113] Cells are placed in the center of the four electrodes (*e.g.*, using laser tweezers). Rotation spectra are obtained by measuring the rotation speed at each frequency over a frequency range of 1 kHz to around 100 MHz. By fitting the rotation spectra, specific membrane capacitance, cytoplasm conductivity and cytoplasm permittivity values are determined.[92,114,115] Fig. 3(b) illustrates the working mechanism of a microfluidic electro-rotation device.[108] The ROT technique has been used to test a number of cell types, such as white blood cells and human cancer cells.[91,92,114–116] Electrorotation is a slow technique. It takes approximately 30 min to test a single cell.[113,117] It is also difficult to achieve efficient rotation in a high conductivity physiological buffer. Hence, electrical properties of the tested cell may have already been altered when immersed in the low conductivity sucrose buffer. Nevertheless, electrorotation is the only method capable of extracting inherent electrical properties of cells, such as membrane permittivity and cytoplasm conductivity. The methodology and electrical models can be instrumental for the development of new techniques for higher throughput.

Table 3 Microfluidic devices for single-cell electrical characterization

	Techniques	Targeted cells	Frequency	Summary	Throughput[a]	Ref.
Coulter counter	Liquid aperture	25 μm particles	50 kHz	A liquid aperture defined by two-dimensional sheath flow prevents clogging and provides a higher accuracy.	N/A	98
	Multiple channels	40 μm particles and 17–23 μm pollen	DC	Coulter counter using multiple channels improved efficiency by 300%.	N/A	99
	Platinum black electroplated electrodes	5.8 and 10 μm particles and blood cells	100 Hz–7 MHz	Platinum black electroplated electrodes reduced the electrical double layer effect by increasing surface area.	N/A	102
	Polyelectrolytic salt bridge-based electrodes	9.95 and 5.7 μm particles; RBCs and WBCs	DC	RBCs and WBCs were distinguished using polyelectrolytic salt bridge-based electrodes.	1000 cells s^{-1}	103
	Polyelectrolytic gel electrodes	7.2, 10.0 and 15.0 μm particles and RBCs	DC	Polyelectrolytic gel electrodes were developed to reduce the electrical double layer effect.	N/A	104
	Tunable sensitivity	*E. coli*	50 kHz	A multi-layered microfluidic device with tunable detection volume enabled a higher sensitivity and dynamic range.	N = hundreds	135
	Polyelectrolytic gel electrodes + focusing	CTCs	DC	CTCs were successfully detected in blood samples from 24 out of 24 breast cancer patients.	N/A	105
Electrorotation	Four electrodes in phase quadrature	WBCs	10 kHz–100 MHz	Leukocyte subpopulations were identified based on their electrical properties.	N = ~220	91
	Four electrodes in phase quadrature	DS19	10 kHz–100 MHz	Specific membrane capacitance is determined by the complexity of surface features.	N = ~200	92
	Four electrodes in phase quadrature	MCF/neo, MCF/HER2-11, MCF/HER2-18	10 kHz–100 MHz	Specific membrane capacitance of various cell lines was reported.	N = 89	113
	Four electrodes in phase quadrature	MDA 231, T-lymphocytes and RBCs	1 kHz–1 GHz	Specific membrane capacitance, cytoplasm conductivity, and cytoplasm permittivity values were reported.	N = 60	115
μ-EIS	Micropillars	HeLa	1 Hz–100 kHz	A circuit model was developed for electrical component calculation.	N/A	118
	Hydraulic trapping	HeLa	300 kHz	Surfactant and bacterial pore-forming toxin effects were investigated using impedance monitoring.	N/A	119
	Vertical hole	MCF-7, MCF-10A, MCF-MB-231 and MDA-MB-435	10 kHz–3 MHz	Impedance spectra were shown to be significantly different between the normal cell lines and each of the cancer cell lines.	7–10 cells/type	120
	Parallel lateral trapping holes	686LN and 686LN-M4e	40 Hz–10 MHz	The phase part of impedances could be used to differentiate the poorly metastatic cell line from the highly metastatic cell line.	N = 129	121
	DEP trapping	HeLa	1 Hz–100 kHz	A DEP force was used to trap cells.	N/A	122
	Vertical hole	L929	1 Hz–1 MHz	A culture of L929 cells and the toxicity effect on impedance measurement are monitored.	N/A	124
	Vertical hole	Arpe-19	1 kHz	The subtoxic effect was measured by monitoring impedance signals over time.	N/A	125

Table 3 (*Continued*)

	Techniques	Targeted cells	Frequency	Summary	Throughput[a]	Ref.
IFC	Coplanar electrodes	Three types of algae	327 kHz and 6.03 MHz	Three populations of algae were distinguished on the basis of impedance measurement.	$N \approx 3392$	128
	Coplanar electrodes	*Babesia bovis*-infected RBCs	8.7 MHz	The real part and imaginary part of the impedance signal were used for cell type classification.	$N = 5900$	136
	Parallel facing electrodes	RBCs, ghost RBCs and fixed RBCs	602 kHz and 10 MHz	Controlled RBCs, ghost RBCs and fixed RBCs were distinguished using impedance opacity.	1000 cells min^{-1}	127
	Parallel facing electrodes	WBCs	573 kHz and 1.7 MHz	Microfluidic impedance flow cytometry was incorporated with fluorescence detection.	$\sim$100 cells s^{-1}	129
	Parallel facing electrodes	Macrophage, MCF-7, RN22, blood cells; bacteria and yeast	0.5 MHz–15 MHz	Macrophage differentiation, cell viability, blood cells, and RN22 with altered membrane potential and intercellular calcium concentration were distinguished.	200–20 000 cells min^{-1}	130
	Parallel facing electrodes	RBCs and WBCs	573 kHz and 1.7 MHz	The functions of blood dilution, RBCs lysis, and hemoglobin detection were integrated.	N/A	131
	Parallel facing electrodes	3T3-L1, Adipocyte and monocyte, Jurkat cell, Yeast cell	624 kHz and 1–15 MHz	Various cell lines, human monocytes and *in vitro*-differentiated dendritic cells and macrophages, viable and apoptotic Jurkat cells were discriminated. Yeast cell growth was also monitored using impedance measurement.	200–1000 cells min^{-1}	137
	Parallel facing electrodes + hydrodynamic focus	*E. coli* and 1,2 μm beads	503 kHz	A focusing technique mitigated the clogging issue and increased sensitivity.	N/A	138
	Liquid electrodes + DEP focusing	Yeast cells	500 kHz and 15 MHz	DEP was applied to reduce measurement variations by focusing particles in the middle of the channel.	N/A	133
	Electrophysiological cytometry	Pluripotent stem cells	N/A	Clusters of undifferentiated human-induced pluripotent stem cells (iPSC) were identified from iPSC-derived cardiomyocyte (iPSC-CM) clusters.	$N = 45$	134
	Constriction channel + 7 frequencies measurement	AML-2 and HL-60	1 kHz–400 kHz	Specific membrane capacitance and cytoplasm conductivity values were determined at a speed of 5–10 cells s^{-1}.	5–10 cells s^{-1}	139

[a] Throughput: For those references that explicitly reported speed/throughput, speed/throughput is listed directly in the table. For those references where speed/throughput was not explicitly reported, we calculated speed/throughput using the data plots (*e.g.*, histograms) presented in those references

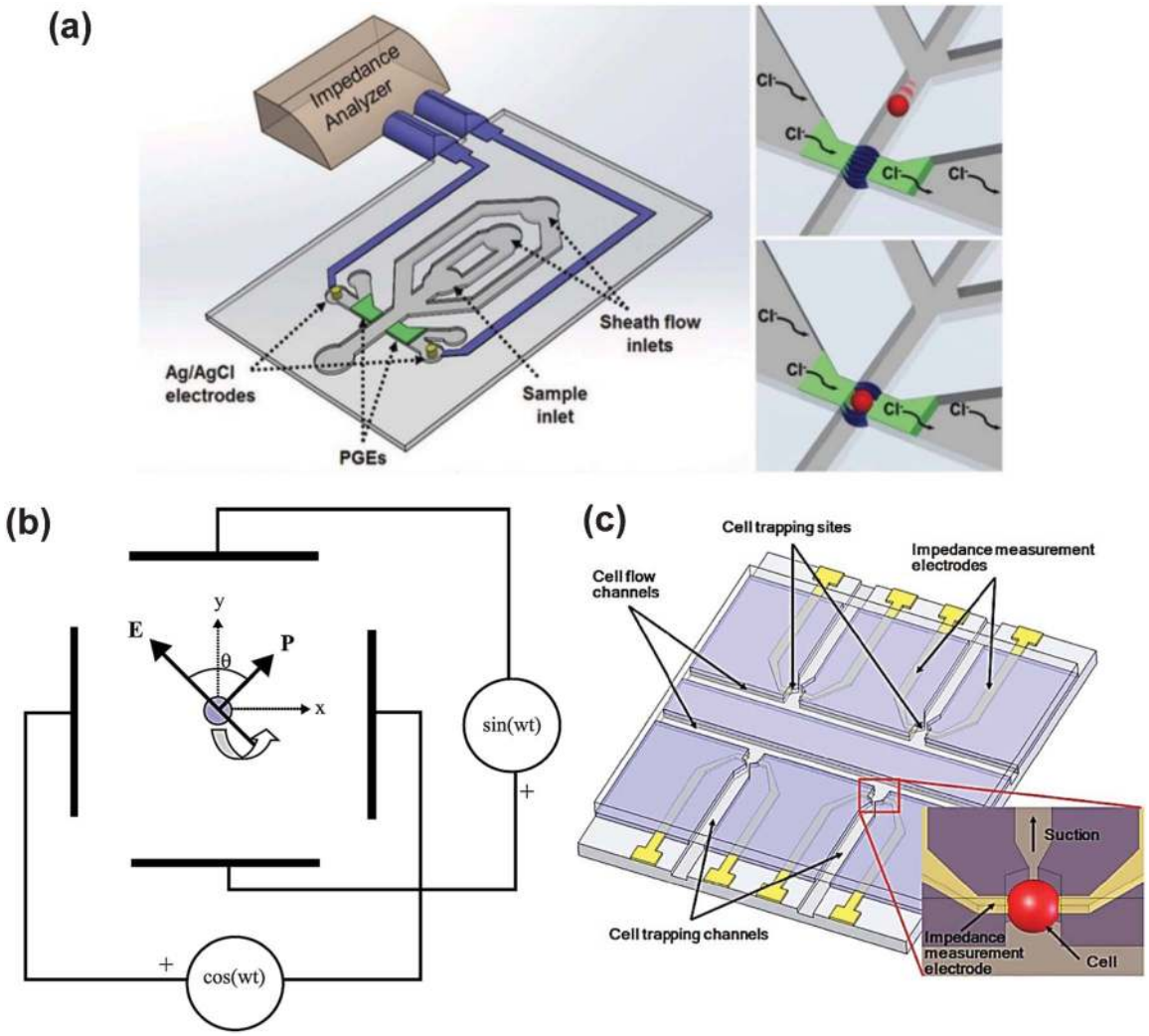

Fig. 3 (a) A schematic illustration of a PGE-based DC impedance cell counter. Ionic flows between the PGEs under low DC bias are interrupted when a cell passes through, causing a DC impedance change. The sheath flow is used for focusing cells and preventing cell adhesion to chambers and channels. Reproduced with permission from ref. 105. (b) Electrorotation. A cell is placed in the center of four micro-electrodes connected in phase quadrature (90° difference) and rotated by the DEP forces generated by the rotating electrical field. Rotation spectra (rotation rate *vs.* frequency) are used to extract the electrical properties of the cells. Reproduced with permission from ref. 108. (c) A schematic representation of the μ-EIS system showing four impedance analysis sites positioned along the two cell flow channels. The close-up view illustrates a single cell trapped inside a cell trap. The trapped cell forms a tight seal with the two integrated electrodes for impedance measurement. Reproduced with permission from ref. 121.

Microelectrical impedance spectroscopy (μ-EIS)

Microelectrical impedance spectroscopy (μ-EIS) is a technique wherein a frequency-dependent excitation signal is applied across a trapped cell to measure the corresponding current response. Various cell trapping mechanisms incorporated with microfabricated electrodes have been proposed, such as hydrodynamic traps,[118,119] negative pressure traps,[120,121] and DEP traps.[122]

Jang *et al.* developed a microfluidic device which utilizes micropillars within a microfluidic channel to physically capture and measure the impedance of a single human cervical epithelioid carcinoma (HeLa) cell using EIS.[118] Hydraulic trapping devices were also demonstrated where impedance measurements were accomplished by recording the current from two electrode pairs, one empty (reference) and one containing a cell. The effect of surfactant and bacterial pore-forming toxins on HeLa cells was monitored continuously.[119] To minimize current leakage, caused by the current undesirably obviating the targeted cell through the low resistivity medium, Cho *et al.* developed an array of planar micro-holes for positioning cells and forming direct contact between cells and electrodes (see Fig. 3(c)).[121] Li *et al.* used a vertical sub-micrometer opening with embedded recording electrodes. The device was capable of reducing the serial resistance, while keeping the seal resistance for high sensitivity measurements.[123] Since single cells can be cultured right on the vertical holes, the capability of monitoring the dynamic changes of singe cell electrical properties over a period of time is a merit of the vertical hole-based technique.[124,125]

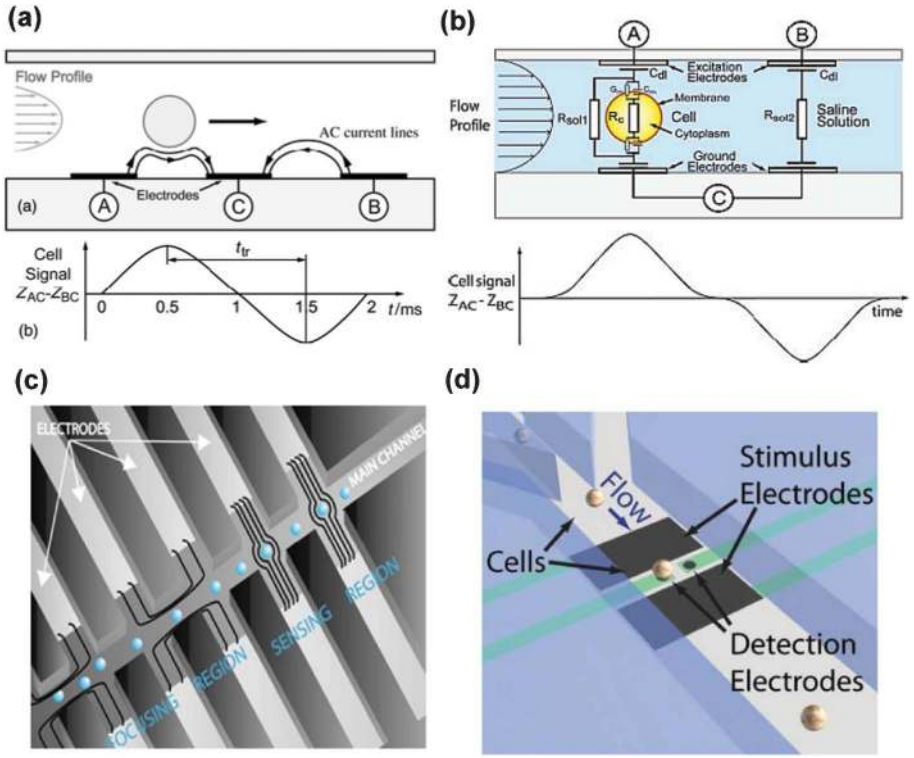

Fig. 4 (a) Impedance flow cytometry with coplanar electrodes. A side view shows a particle passing over three electrodes (A, C, and B). The impedance signal is measured differentially (Z_{AC}–Z_{BC}). Reproduced with permission from ref. 126. (b) Impedance flow cytometry with parallel facing electrodes. A side view shows a cell passing between the measurement and reference electrodes. Reproduced with permission from ref. 127. (c) Impedance flow cytometry combining impedance measurements and dielectrophoretic focusing. Reproduced with permission from ref. 133. (d) Label-free electrophysiological cytometry. Electrodes are integrated for both electrical stimulation of cells and recording of their extracellular field potential signals. Reproduced with permission from ref. 134.

There are two major limitations of the μ-EIS technique. Firstly, since the trapping and releasing process is time consuming, and the measurement of impedance spectra also takes time, the throughput of μ-EIS is low. Only tens of cells were tested in reported studies. Secondly, although the capacitance and resistance of tested cells can be determined by interpreting impedance spectra with electrical models, these parameters are strongly affected by electrode size, the cell trapping mechanism, cell volume and the interaction with other cells (*vs.* size-independent parameters, such as specific membrane capacitance and cytoplasm conductivity).

Impedance flow cytometry (IFC)

Although the Coulter counter has become a widely used technique in clinical instruments (*e.g.*, hematology analyzers), the conventional Coulter counter is only capable of classifying cell types that have distinct volume differences. Some of the most recent commercial hematology analyzers adopted both DC and RF measurements. The ratio of the RF signal to the DC signal is defined as opacity, which is used as a volume independent electrical signature of the tested cells. Along with the DC signal (volume signature), a WBC differentials count can be achieved. This technique was recently demonstrated on microfluidic devices. In addition to WBC count, microfluidic flow cytometry has also been used for analyzing a variety of particles.[126–130]

An impedance flow cytometry design using coplanar electrodes was demonstrated by Gawad *et al.*[126] As shown in Fig. 4(a), three microfabricated electrodes were integrated on the bottom of the microfluidic channel. When microparticles were flowing through the detection area, the impedance change was recorded differentially. The non-uniform electrical field distribution in the channel, resulting in positional variations of tested cells, may undesirably affect impedance measurement. To overcome this issue, parallel facing electrodes were developed (see Fig. 4(b)).[127] When a cell is present in between one pair of electrodes, the other pair is used as a reference, allowing the differential measurement of electrical signals. The device was demonstrated to be capable of detecting electrical property differences between normal RBCs and glutaraldehyde-fixed RBCs.

Holmes *et al.* incorporated a fluorescence measurement unit on their microfluidic flow cytometry device.[129] This device design enabled direct correlation of impedance signals from individual cells with their biochemical phenotypes. A 3-part WBC differential count of human blood was well achieved. The same group more recently developed a microfluidic impedance flow cytometry device integrated with RBC lysis and a hemoglobin concentration measurement unit.[131,132] Besides counting blood cells, microfluidic impedance flow cytometry has also found applications in other areas, such as the measurement of cell viability and physiological differences of

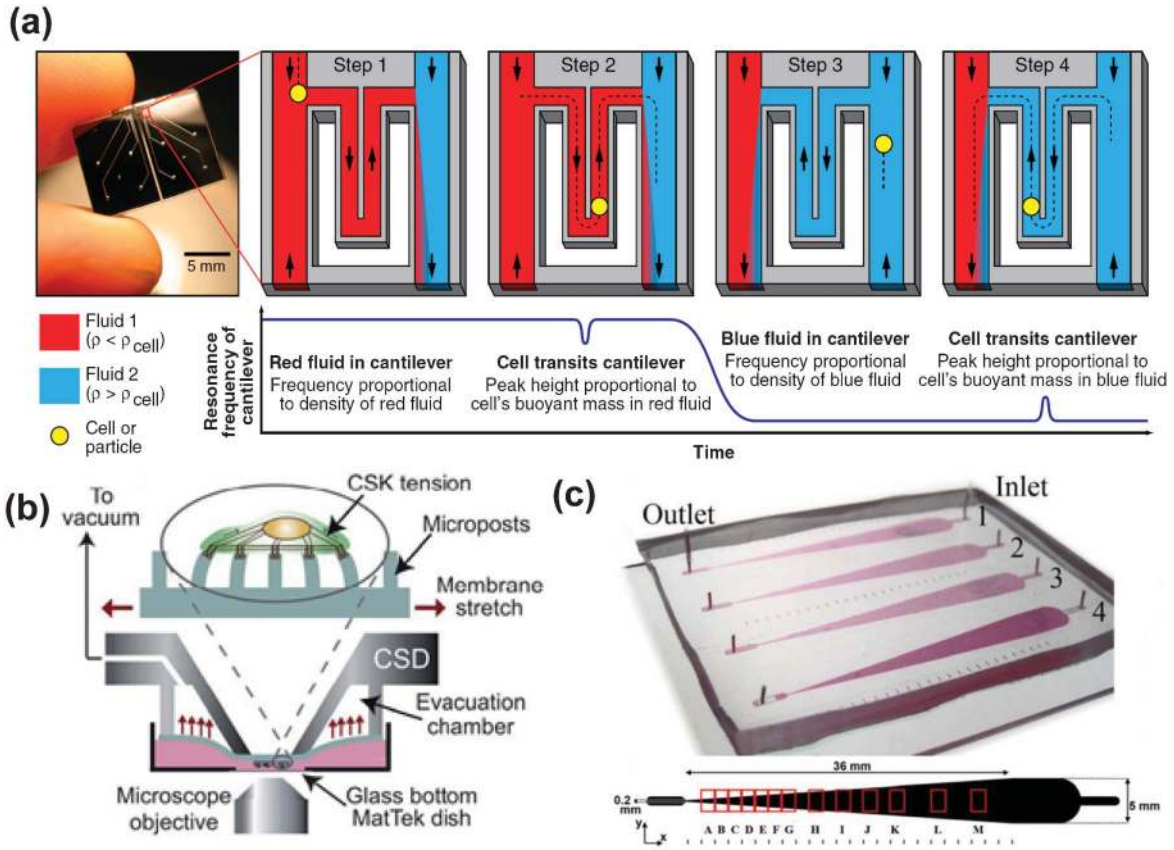

Fig. 5 (a) Suspended microchannel resonator for single-cell density measurement. The buoyant mass of the cell was recorded in two fluids of different densities. The red fluid is less dense than the cell, while the blue fluid has a higher density than the cell. From the resonance frequency shift, absolute mass and density are determined. Reproduced with permission from ref. 33. (b) A cell stretching device containing a micropost array membrane to modulate equibiaxial cell stretching, while simultaneously measuring live-cell subcellular contractile response. A vacuum could be drawn in the evacuation chamber to stretch the micropost array over the viewing aperture. Reproduced with permission from ref. 152. (c) A microfluidic device with four independent branches for cell adhesion measurement. Tapered channels are used to explore a range of shear stresses along the channel. The colored rectangles are the visual fields of different shear stress zones. Reproduced with permission from ref. 158.

cells.[130] More details on impedance flow cytometry can be found elsewhere.[112,130] In addition to coplanar and parallel facing electrode designs, Mernier *et al.* demonstrated "liquid electrodes" to discriminate living and dead yeast cells (see Fig. 4(c)). The larger electrodes recessed in lateral channels allow measurements at low frequencies (down to 1 kHz), and the same "liquid electrodes" can also be used for DEP focussing of the particles.[133] Recently, the concept of label-free electrophysiological cytometry was reported. This technique utilizes the nature of electrically-excitable cells (upon activation by sufficient transmembrane electric fields, different cell types generate different extracellular field potential signals) to distinguish different cell types. As shown in Fig. 4(d), the device is integrated with electrodes for both electrical stimulation and recording of extracellular field potential signals from suspended cells in flow.[134] Undifferentiated human-induced pluripotent stem cells (iPSC) and iPSC-derived cardiomyocyte (iPSC-CM) cells were distinguished.

Other physical characterization techniques

While clinical applications have been mostly driving the development of microfluidic tools for single-cell biophysical characterization, these new tools are also enabling biologists to gain insights into the cell development process. For instance, the microfluidic device reported in ref. 140 for the first time enabled the measurement of the mass of microparticles. When particles suspended in liquid flow through nanomechanical resonators, the resulting frequency shift is used to determine the mass of the particles with extraordinary sensitivity (10^{-21} g). Combined with microfluidic control, the 'instantaneous' growth rates of individual cells were determined,[141] and it was found that heavier cells grew faster than lighter cells. Using this technology, the density of single living cells was also measured.[33] As shown in Fig. 5(a), the suspended microfluidic resonator consists of a silicon cantilever and an embedded microfluidic channel. When cells flow through the microfluidic channel, the changes in resonance frequency are proportional to the buoyant mass of the cell. In order to measure the density of the cell, the

buoyant mass of the targeted single cells was recorded in two fluids of different densities. The absolute mass and density were then determined and were used to distinguish malaria-infected RBCs, RBCs from patients with sickle cell disease and thalassemia, and drug-treated leukemia cells. The microfluidic system has a testing speed of $\sim$500 cells h^{-1}.

Compressive forces can be applied directly to cells through a mechanism similar to bulging elastomeric valves.[142] In general, such devices consist of multiple layers and a thin elastomeric membrane separating the flow and control channels. The cells within the flow channels are compressed when a pneumatic pressure is applied to deflect the thin membrane. Microfluidic devices based on the compression have been used to monitor cell viability and induce mechanical cell lysis of adherent breast cancer cells (MCF-7).[143] A more recent study by Kim *et al.* has shown that under excessive deformation of the deflecting membrane, small morphological changes known as ''bulges'' occur on the cellular membrane as a result of local detachment of the cytoskeleton lipid bilayer. In addition, differences in the uniformity of bulge distribution on the cell's periphery can be used as a physical indicator to distinguish different cells.[144] A similar technology can also be used for viscoelastic characterization of cells of a small population in suspension. Du *et al.* estimated global viscoelastic time constants of the HL-60 cell line and 3T3 fibroblasts by observing the recovery time upon the removal of the compression force.[145] This design can also be extended to the mechanical characterization of other specimens, such as biofilms.[146] Alternatively, hydrostatic pressure can apply a uniform compressive force without physical contact.[147]

Micropost arrays have been used to measure the traction force generated by a cell at the adhesion sites.[148] The force applied by the cell to the substrate was calculated down to the level of a single adhesion site, based on the visualization of displacements and locations of the focal adhesions.[148] Tan *et al.* used microfabricated microposts to determine mechanical cell–substrate interactions. By varying the geometry of the microposts, cell adhesion was controlled, and the results revealed that the magnitude of the traction force generated by the cell was regulated by its morphology.[149] Schoen *et al.* investigated the effect of elastic substrate warping on force measurements. A correction factor was analytically and experimentally determined, which allows for a more accurate comparison of absolute forces between different pillar geometries and designs.[150] In order to separately study the cellular response to external forces applied to a cell, and the internal forces generated by the cell, magnetic microposts containing cobalt nanowires that can be actively manipulated were developed.[151] Fu and co-workers devised a strategy involving an array of microposts integrated onto a stretchable elastomeric membrane, enabling simultaneous stretching and contractile response monitoring of vascular smooth muscle cells[152] (see Fig. 5(b)).

Due to the micro-scale dimensions of microfluidic channels, microchannels are suitable for generating fluid shear forces to study the substrate adhesion strength of cells. Several studies have quantified the adhesion strength of mammalian fibroblasts.[153–155] These microfluidic devices share the commonalities of using microchannels with a protein coating to alter cell adhesion, which is tested under shearing fluid flow. Channels with varying widths were also developed to quantify cell adhesion strength.[155,156] Using a similar tapered design, Gutierrez *et al.* demonstrated that activated neutrophils had a greater adhesion strength than their non-activated counterparts,[157] and Rupprecht *et al.* used a tapered channel to quantify the adhesion strength of human breasts cancer cells[158] (see Fig. 5(c)).

Outlooks

For clinical applications, cell samples from pleural fluid, urine and blood are highly heterogeneous, and the number of cells of interest is usually low (*e.g.*, CTC cells). Thus, low-throughput techniques that are only able to test tens or hundreds of cells have little clinical relevance. In order to obtain statistically meaningful data, testing a large number of cells is necessary. Several techniques are able to provide reasonable throughput. For example, the constriction-channel device reported in ref. 39 achieved 100–150 cells s^{-1} and is capable of performing multi-parameter measurements. Since the measurements are completely electrical, by refining experimental parameters, a further increase in throughput could be feasibly achievable. The hydrodynamic stretching microfluidic device reported in ref. 19 has proven its clinical relevance and can provide a testing speed of approximately 2000 cells s^{-1}. Although high-speed image recording and image analysis are a bottleneck, rapid advances in the imaging industry and hardware-based image processing could further enhance the clinical relevance of the microfluidic deformability cytometry technique.[159] Besides throughput, one challenge for microfluidic cell deformability measurements presently lies in the weak correlation between cell deformability and the widely used biochemical markers. An intrinsic connection between pathological cell deformability changes and their biochemical/molecular changes must be well established before cell deformability can practically be accepted as a clinical marker.

Cell deformability changes in response to environmental factors also needs to be better understood. After cells are harvested from the incubating environment or retrieved from the human body, the deformability of the cells starts to change. Many environmental parameters, such as temperature, CO_2 concentration, and osmotic pressure, can have an influence on the deformability change. Thus, for cell deformability testing, testing conditions should be maintained as consistently as possible, and all cells should be tested within a strictly defined period of time. Establishing a standard testing protocol is necessary as microfluidic cell deformability testing moves towards clinical applications.

As for electrical measurements, microfluidic impedance flow cytometry appears promising since the conventional Coulter counter is a well-accepted technology. The DC/RF

measurement technique has proven effective for clinical WBC differential count and is used in some commercial hematology analyzers. Thus, clinical acceptance and commercial success of microfluidic impedance flow cytometry could be achievable. As a precursor, instruments based on a miniaturized Coulter counter have entered the market. For instance, Chempaq (UNITECH, Denmark) is a portable hematology analyzer capable of 3-part WBC differential count, RBC count, and hemoglobin concentration measurements. Finger prick blood is loaded onto a disposable cassette, in which an aperture is placed. Only DC measurement is conducted by the instrument, and a 3-part WBC differential count is based on the modification of cell volume from chemical treatment.

Microfluidic impedance flow cytometry has proven more powerful than the microfluidic Coulter counter. Microfluidic impedance flow cytometry has been demonstrated to distinguish cells based on their physiological and pathological conditions, such as viability and membrane potential change.[130] Although it is known that electrical properties of cells can possibly be used for distinguishing cell types (*e.g.*, benign and malignant tumor cells), the establishment of the connections between cell physiological changes and their electrical properties has not gained as much interest as cell deformability research, likely due to the lack of powerful tools for cellular electrical characterization. Among the techniques discussed earlier in this review, only electrorotation is capable of quantifying a cell's intrinsic (size and shape-independent) electrical properties (*e.g.*, specific membrane capacitance and cytoplasm conductivity). However, electrorotation's testing throughput is too low to generate meaningful results for diagnostic applications. Microfluidic impedance flow cytometry[127,130–132] that uses opacity (ratio of high-frequency amplitude/low-frequency amplitude) as the indicator of a cell's electrical properties can offer a high throughput. Opacity is a combined effect of the cell membrane and cytoplasm. A single RF frequency must be selected carefully so that different electrical properties of the cell membrane and/or cytoplasm can be well reflected in the opacity value. It is difficult to correlate electrical properties to physiological changes of cells since the opacity value can only reflect the electrical property changes of the cells. It cannot tell you what has caused the difference in opacity values and how the electrical properties have changed. In order to tackle this challenge, we recently reported a microfluidic device, which is capable of quantifying inherent electrical properties (specific membrane capacitance and cytoplasm conductivity) of single cells at a reasonable testing speed of 5–10 cells s^{-1} (*vs.* minutes per cell using existing techniques, such as electrorotation).[139] Impedance profiles at seven frequencies were measured simultaneously when cells were aspirated through a constriction channel. Based on the geometrical and electrical models, specific membrane capacitance and cytoplasm conductivity values of over 6000 HL-60 and AML-2 cells were quantified.

In summary, we highlighted the recent developments of microfluidics-based techniques for the characterization of biophysical properties of single cells. Compared with conventional single-cell biophysical characterization tools, microfluidic devices have demonstrated great potential in realizing multi-parameter measurements on single cells at a higher testing speed. Biophysical measurements as a label-free approach can potentially be used for disease prescreening. For example, if biophysical measurements on cells indicate possible diseases, further clinical examinations can be done to evaluate the disease condition. Biophysical measurements can also be incorporated with a cell sorting unit to collect cells having different physical properties for further biochemical assaying.

While the throughput, sensitivity, and specificity of microfluidic biophysical characterization devices still await improvement, biophysical measurements on single cells already prove useful to provide bolstering information to biochemical measurements. Several microfluidic systems combining biophysical and biochemical measurements have been developed to capture multi-parameter information of the target cells.[23,160,161] In the foreseeable future, closer correlations between biophysical and biochemical properties of cells will be established, and advances in microfluidics-based biophysical measurement techniques will move closer to practical applications and enable more discoveries in biology research. Meanwhile, as microfluidic devices for single-cell biophysical characterization are more integrated, compact, and easy-to-use, they can potentially become clinically accepted point-of-care tools.

Acknowledgements

Financial support from the Natural Sciences and Engineering Research Council of Canada (NSERC) through an NSERC Steacie Fellowship, from the University of Toronto through a Connaught Innovation Award, and from the Canada Research Chairs Program is acknowledged.

References

1 J. El-Ali, P. K. Sorger and K. F. Jensen, Cells on chips, *Nature*, 2006, **442**, 403–411.
2 A. Fritsch, M. Hockel, T. Kiessling, K. D. Nnetu, F. Wetzel, M. Zink and J. A. Kas, Are biomechanical changes necessary for tumour progression?, *Nat. Phys.*, 2010, **6**, 730–732.
3 C. Moraes, Y. Sun and C. A. Simmons, (Micro)managing the mechanical microenvironment, *Integr. Biol.*, 2011, **3**, 959–971.
4 S. Suresh, Biomechanics and biophysics of cancer cells, *Acta Biomater.*, 2007, **3**, 413–438.
5 J. Chen, J. Li and Y. Sun, Microfluidic approaches for cancer cell detection, characterization, and separation, *Lab Chip*, 2012, **12**, 1753–1767.
6 S. I. Kim and H. I. Jung, Circulating Tumor Cells: Detection Methods and Potential Clinical Application in Breast Cancer, *J. Breast Cancer*, 2010, **13**, 125–131.

7 G. Y. H. Lee and C. T. Lim, Biomechanics approaches to studying human diseases, *Trends Biotechnol.*, 2007, **25**, 111–118.
8 S. E. Cross, Y. S. Jin, J. Rao and J. K. Gimzewski, Nanomechanical analysis of cells from cancer patients, *Nat. Nanotechnol.*, 2007, **2**, 780–783.
9 H. Morgan, T. Sun, D. Holmes, S. Gawad and N. G. Green, Single cell dielectric spectroscopy, *J. Phys. D: Appl. Phys.*, 2007, **40**, 61–70.
10 R. N. Zare and S. Kim, Microfluidic Platforms for Single-Cell Analysis, *Annu. Rev. Biomed. Eng.*, 2010, **12**, 187–201.
11 G. M. Whitesides, The origins and the future of microfluidics, *Nature*, 2006, **442**, 368–373.
12 S. A. Vanapalli, M. H. G. Duits and F. Mugele, Microfluidics as a functional tool for cell mechanics, *Biomicrofluidics*, 2009, **3**, 012006.
13 D. H. Kim, P. K. Wong, J. Park, A. Levchenko and Y. Sun, Microengineered Platforms for Cell Mechanobiology, *Annu. Rev. Biomed. Eng.*, 2009, **11**, 203–233.
14 Y. Zheng and Y. Sun, Microfluidic devices for mechanical characterisation of single cells in suspension, *Micro Nano Lett.*, 2011, **6**, 327–331.
15 A. W. L. Jay, Viscoelastic properties of the human red blood cell membrane. I. Deformation, volume loss, and rupture of red cells in micropipettes, *Biophys. J.*, 1973, **13**, 1166–1182.
16 R. Skalak and Branemar Pi, Deformation of Red Blood Cells in Capillaries, *Science*, 1969, **164**, 177.
17 M. Diez-Silva, M. Dao, J. Y. Han, C. T. Lim and S. Suresh, Shape and Biomechanical Characteristics of Human Red Blood Cells in Health and Disease, *MRS Bull.*, 2010, **35**, 382–388.
18 M. Makale, Cellular mechanobiology and cancer metastasis, *Birth Defects Res., Part C*, 2007, **81**, 329–343.
19 D. R. Gossett, H. T. K. Tse, S. A. Lee, Y. Ying, A. G. Lindgren, O. O. Yang, J. Rao, A. T. Clark and D. Di Carlo, Hydrodynamic stretching of single cells for large population mechanical phenotyping, *Proc. Natl. Acad. Sci. U. S. A.*, 2012, **109**, 7630–7635.
20 D. Di Carlo, A Mechanical Biomarker of Cell State in Medicine, *JALA*, 2012, **17**, 32–42.
21 F. Lautenschlager, S. Paschke, S. Schinkinger, A. Bruel, M. Beil and J. Guck, The regulatory role of cell mechanics for migration of differentiating myeloid cells, *Proc. Natl. Acad. Sci. U. S. A.*, 2009, **106**, 15696–15701.
22 J. P. Shelby, J. White, K. Ganesan, P. K. Rathod and D. T. Chiu, Amicrofluidic model for single-cell capillary obstruction by Plasmodium falciparum infected erythrocytes, *Proc. Natl. Acad. Sci. U. S. A.*, 2003, **100**, 14618–14622.
23 H. Bow, I. V. Pivkin, M. Diez-Silva, S. J. Goldfless, M. Dao, J. C. Niles, S. Suresh and J. Y. Han, A microfabricated deformability-based flow cytometer with application to malaria, *Lab Chip*, 2011, **11**, 1065–1073.
24 J. P. Mills, M. Diez-Silva, D. J. Quinn, M. Dao, M. J. Lang, K. S. W. Tan, C. T. Lim, G. Milon, P. H. David, O. Mercereau-Puijalon, S. Bonnefoy and S. Suresh, Effect of plasmodial RESA protein on deformability of human red blood cells harboring Plasmodium falciparum, *Proc. Natl. Acad. Sci. U. S. A.*, 2007, **104**, 9213–9217.
25 Y. K. Park, M. Diez-Silva, G. Popescu, G. Lykotrafitis, W. S. Choi, M. S. Feld and S. Suresh, Refractive index maps and membrane dynamics of human red blood cells parasitized by Plasmodium falciparum, *Proc. Natl. Acad. Sci. U. S. A.*, 2008, **105**, 13730–13735.
26 S. Eber and S. E. Lux, Hereditary spherocytosis-Defects in proteins that connect the membrane skeleton to the lipid bilayer, *Semin. Hematol.*, 2004, **41**, 118–141.
27 S. Perrotta, P. G. Gallagher and N. Mohandas, Hereditary spherocytosis, *Lancet*, 2008, **372**, 1411–1426.
28 L. D. Walensky, M. Narla and S. E. Lux, *Blood: principles and practice of hematology*, Lippincott Williams and Wilkins, Philadelphia, 2003.
29 S. K. Ballas and E. D. Smith, Red-Blood-Cell Changes during the Evolution of the Sickle-Cell Painful Crisis, *Blood*, 1992, **79**, 2154–2163.
30 G. A. Barabino, M. O. Platt and D. K. Kaul, Sickle Cell Biomechanics, *Annu. Rev. Biomed. Eng.*, 2010, **12**, 345–367.
31 O. K. Baskurt, D. Gelmont and H. J. Meiselman, Red blood cell deformability in sepsis, *Am. J. Respir. Crit. Care Med.*, 1998, **157**, 421–427.
32 T. C. Hurd, K. S. Dasmahapatra, B. F. Rush and G. W. Machiedo, Red Blood-Cell Deformability in Human and Experimental Sepsis, *Arch. Surg.*, 1988, **123**, 217–220.
33 W. H. Grover, A. K. Bryan, M. Diez-Silva, S. Suresh, J. M. Higgins and S. R. Manalis, Measuring single-cell density, *Proc. Natl. Acad. Sci. U. S. A.*, 2011, **108**, 10992–10996.
34 C. D. Brown, H. S. Ghali, Z. H. Zhao, L. L. Thomas and E. A. Friedman, Association of reduced red blood cell deformability and diabetic nephropathy, *Kidney Int.*, 2005, **67**, 295–300.
35 S. Keymel, C. Heiss, P. Kleinbongard, M. Kelm and T. Lauer, Impaired Red Blood Cell Deformability in Patients with Coronary Artery Disease and Diabetes Mellitus, *Horm. Metab. Res.*, 2011, **43**, 760–765.
36 K. Tsukada, E. Sekizuka, C. Oshio and H. Minamitani, Direct measurement of erythrocyte deformability in diabetes mellitus with a transparent microchannel capillary model and high-speed video camera system, *Microvasc. Res.*, 2001, **61**, 231–239.
37 E. Bennett-Guerrero, T. H. Veldman, A. Doctor, M. J. Telen, T. L. Ortel, T. S. Reid, M. A. Mulherin, H. Zhu, R. D. Buck, R. M. Califf and T. J. McMahon, Evolution of adverse changes in stored RBCs, *Proc. Natl. Acad. Sci. U. S. A.*, 2007, **104**, 17063–17068.
38 J. Bonaventura, Clinical implications of the loss of vasoactive nitric oxide during red blood cell storage, *Proc. Natl. Acad. Sci. U. S. A.*, 2007, **104**, 19165–19166.
39 Y. Zheng, E. Shojaei-Baghini, A. Azad, C. Wang and Y. Sun, High-throughput biophysical measurement of human red blood cells, *Lab Chip*, 2012, **12**, 2560–2567.
40 W. G. Lee, H. Bang, H. Yun, J. Lee, J. Park, J. K. Kim, S. Chung, K. Cho, C. Chung, D. C. Han and J. K. Chang, On-chip erythrocyte deformability test under optical pressure, *Lab Chip*, 2007, **7**, 516–519.
41 S. C. Gifford, M. G. Frank, J. Derganc, C. Gabel, R. H. Austin, T. Yoshida and M. W. Bitensky, Parallel microchannel-based measurements of individual erythrocyte areas and volumes, *Biophys. J.*, 2003, **84**, 623–633.

42 S. C. Gifford, J. Derganc, S. S. Shevkoplyas, T. Yoshida and M. W. Bitensky, A detailed study of time-dependent changes in human red blood cells: from reticulocyte maturation to erythrocyte senescence, *Br. J. Haematol.*, 2006, **135**, 395–404.
43 T. Herricks, M. Antia and P. K. Rathod, Deformability limits of Plasmodium falciparum-infected red blood cells, *Cell. Microbiol.*, 2009, **11**, 1340–1353.
44 M. Abkarian, M. Faivre and H. A. Stone, High-speed microfluidic differential manometer for cellular-scale hydrodynamics, *Proc. Natl. Acad. Sci. U. S. A.*, 2006, **103**, 538–542.
45 M. J. Rosenbluth, W. A. Lam and D. A. Fletcher, Analyzing cell mechanics in hematologic diseases with microfluidic biophysical flow cytometry, *Lab Chip*, 2008, **8**, 1062–1070.
46 H. W. Hou, Q. S. Li, G. Y. H. Lee, A. P. Kumar, C. N. Ong and C. T. Lim, Deformability study of breast cancer cells using microfluidics, *Biomed. Microdevices*, 2009, **11**, 557–564.
47 J. Chen, Y. Zheng, Q. Y. Tan, E. Shojaei-Baghini, Y. L. Zhang, J. Li, P. Prasad, L. D. You, X. Y. Wu and Y. Sun, Classification of cell types using a microfluidic device for mechanical and electrical measurement on single cells, *Lab Chip*, 2011, **11**, 3174–3181.
48 A. Adamo, A. Sharei, L. Adamo, B. Lee, S. Mao and K. F. Jensen, Microfluidics-based assessment of cell deformability, *Anal. Chem.*, 2012, **84**, 6438–6443.
49 G. Guan, P. C. Y. Chen, W. K. Peng, A. A. Bhagat, C. J. Ong and J. Han, Real-time control of a microfluidic channel for size-independent deformability cytometry, *J. Micromech. Microeng.*, 2012, **22**, 105037.
50 A. M. Forsyth, J. D. Wan, W. D. Ristenpart and H. A. Stone, The dynamic behavior of chemically "stiffened" red blood cells in microchannel flows, *Microvasc. Res.*, 2010, **80**, 37–43.
51 S. S. Lee, Y. Yim, K. H. Ahn and S. J. Lee, Extensional flow-based assessment of red blood cell deformability using hyperbolic converging microchannel, *Biomed. Microdevices*, 2009, **11**, 1021–1027.
52 A. M. Forsyth, J. Wan, P. D. Owrutsky, M. Abkarian and H. A. Stone, Multiscale approach to link red blood cell dynamics, shear viscosity, and ATP release, *Proc. Natl. Acad. Sci. U. S. A.*, 2011, **108**, 10986–10991.
53 W. Bishara, T. W. Su, A. F. Coskun and A. Ozcan, Lensfree on-chip microscopy over a wide field-of-view using pixel super-resolution, *Opt. Express*, 2010, **18**, 11181–11191.
54 X. Q. Cui, L. M. Lee, X. Heng, W. W. Zhong, P. W. Sternberg, D. Psaltis and C. H. Yang, Lensless high-resolution on-chip optofluidic microscopes for Caenorhabditis elegans and cell imaging, *Proc. Natl. Acad. Sci. U. S. A.*, 2008, **105**, 10670–10675.
55 A. Greenbaum, W. Luo, T. W. Su, Z. Gorocs, L. Xue, S. O. Isikman, A. F. Coskun, O. Mudanyali and A. Ozcan, Imaging without lenses: achievements and remaining challenges of wide-field on-chip microscopy, *Nat. Methods*, 2012, **9**, 889–895.
56 S. O. Isikman, W. Bishara, H. Y. Zhu and A. Ozcan, Optofluidic Tomography on a Chip, *Appl. Phys. Lett.*, 2011, **98**, 161109.
57 W. K. Purves, *Life: The Science of Biology*, Sinauer Associates, 6th edn, 2001.
58 J. Kim, I. Hwang, D. Britain, T. D. Chung, Y. Sun and D. H. Kim, Microfluidic approaches for gene delivery and gene therapy, *Lab Chip*, 2011, **11**, 3941–3948.
59 S. Movahed and D. Li, Microfluidics cell electroporation, *Microfluid. Nanofluid.*, 2011, **10**, 703–734.
60 E. Ferret, C. Evrard, A. Foucal and P. Gervais, Volume changes of isolated human K562 leukemia cells induced by electric field pulses, *Biotechnol. Bioeng.*, 2000, **67**, 520–528.
61 N. Bao, Y. H. Zhan and C. Lu, Microfluidic electroporative flow cytometry for studying single-cell biomechanics, *Anal. Chem.*, 2008, **80**, 7714–7719.
62 N. Bao, T. T. Le, J. X. Cheng and C. Lu, Microfluidic electroporation of tumor and blood cells: observation of nucleus expansion and implications on selective analysis and purging of circulating tumor cells, *Integr. Biol.*, 2010, **2**, 113–120.
63 N. Bao, G. C. Kodippili, K. M. Giger, V. M. Fowler, P. S. Low and C. Lu, Single-cell electrical lysis of erythrocytes detects deficiencies in the cytoskeletal protein network, *Lab Chip*, 2011, **11**, 3053–3056.
64 B. E. Henslee, A. Morss, X. Hu, G. P. Lafyatis and L. J. Lee, Electroporation Dependence on Cell Size: Optical Tweezers Study, *Anal. Chem.*, 2011, **83**, 3998–4003.
65 A. Ashkin, Acceleration and Trapping of Particles by Radiation Pressure, *Phys. Rev. Lett.*, 1970, **24**, 156.
66 J. Guck, R. Ananthakrishnan, T. J. Moon, C. C. Cunningham and J. Kas, Optical deformability of soft biological dielectrics, *Phys. Rev. Lett.*, 2000, **84**, 5451–5454.
67 J. Guck, R. Ananthakrishnan, H. Mahmood, T. J. Moon, C. C. Cunningham and J. Kas, The optical stretcher: A novel laser tool to micromanipulate cells, *Biophys. J.*, 2001, **81**, 767–784.
68 E. Jonietz, MECHANICS: The forces of cancer, *Nature*, 2012, **491**, S56–S57.
69 B. Lincoln, H. M. Erickson, S. Schinkinger, F. Wottawah, D. Mitchell, S. Ulvick, C. Bilby and J. Guck, Deformability-based flow cytometry, *Cytometry, Part B*, 2004, **59A**, 203–209.
70 J. Guck, S. Schinkinger, B. Lincoln, F. Wottawah, S. Ebert, M. Romeyke, D. Lenz, H. M. Erickson, R. Ananthakrishnan, D. Mitchell, J. Kas, S. Ulvick and C. Bilby, Optical deformability as an inherent cell marker for testing malignant transformation and metastatic competence, *Biophys. J.*, 2005, **88**, 3689–3698.
71 C. W. Lai, S. K. Hsiung, C. L. Yeh, A. Chiou and G. B. Lee, A cell delivery and pre-positioning system utilizing microfluidic devices for dual-beam optical trap-and-stretch, *Sens. Actuators, B*, 2008, **135**, 388–397.
72 N. Bellini, K. C. Vishnubhatla, F. Bragheri, L. Ferrara, P. Minzioni, R. Ramponi, I. Cristiani and R. Osellame, Femtosecond laser fabricated monolithic chipfor optical trapping and stretching of single cells, *Opt. Express*, 2010, **18**, 4679–4688.
73 F. Bragheri, L. Ferrara, N. Bellini, K. C. Vishnubhatla, P. Minzioni, R. Ramponi, R. Osellame and I. Cristiani, Optofluidic chip for single cell trapping and stretching fabricated by a femtosecond laser, *J. Biophotonics*, 2010, **3**, 234–243.
74 T. W. Remmerbach, F. Wottawah, J. Dietrich, B. Lincoln, C. Wittekind and J. Guck, Oral cancer diagnosis by

mechanical phenotyping, *Cancer Res.*, 2009, **69**, 1728–1732.
75 J. Voldman, Electrical forces for microscale cell manipulation, *Annu. Rev. Biomed. Eng.*, 2006, **8**, 425–454.
76 R. Pethig, Dielectrophoresis: Status of the theory, technology, and applications (vol 4, 022811, 2010), *Biomicrofluidics*, 2010, **4**, 022811.
77 L. A. MacQueen, M. D. Buschmann and M. R. Wertheimer, Mechanical properties of mammalian cells in suspension measured by electro-deformation, *J. Micromech. Microeng.*, 2010, **20**, 065007.
78 J. Chen, M. Abdelgawad, L. M. Yu, N. Shakiba, W. Y. Chien, Z. Lu, W. R. Geddie, M. A. S. Jewett and Y. Sun, Electrodeformation for single cell mechanical characterization, *J. Micromech. Microeng.*, 2011, **21**, 054012.
79 I. Doh, W. C. Lee, Y. H. Cho, A. P. Pisano and F. A. Kuypers, Deformation measurement of individual cells in large populations using a single-cell microchamber array chip, *Applied Physics Letters*, 2012, **100**, 173702.
80 R. M. Hochmuth, Micropipette aspiration of living cells, *J. Biomech.*, 2000, **33**, 15–22.
81 Q. Guo, S. J. Reiling, P. Rohrbach and H. S. Ma, Microfluidic biomechanical assay for red blood cells parasitized by Plasmodium falciparum, *Lab Chip*, 2012, **12**, 1143–1150.
82 J. Chen, Y. Zheng, Q. Y. Tan, Y. L. Zhang, J. Li, W. R. Geddie, M. A. S. Jewett and Y. Sun, A microfluidic device for simultaneous electrical and mechanical measurements on single cells, *Biomicrofluidics*, 2011, **5**, 014113.
83 Y. Katsumoto, K. Tatsumi, T. Doi and K. Nakabe, Electrical classification of single red blood cell deformability in high-shear microchannel flows, *Int. J. Heat Fluid Flow*, 2010, **31**, 985–995.
84 J. Nilsson, M. Evander, B. Hammarstrom and T. Laurell, Review of cell and particle trapping in microfluidic systems, *Anal. Chim. Acta*, 2009, **649**, 141–157.
85 D. R. Gossett, W. M. Weaver, A. J. Mach, S. C. Hur, H. T. K. Tse, W. Lee, H. Amini and D. Di Carlo, Label-free cell separation and sorting in microfluidic systems, *Anal. Bioanal. Chem.*, 2010, **397**, 3249–3267.
86 R. Hoeber, Eine Methode die elektrische Leitfaehigkeit im Innern von Zellen zu messen, *Pfluegers Arch.*, 1910, **133**, 237–259.
87 R. Hoeber, Ein zweites Verfahren die Leitfaehigkeit im Innern von Zellen zu messen, *Pfluegers Arch.*, 1912, **148**, 189–221.
88 R. Hoeber, Messungen der inneren Leitfaehigkeit von Zellen III, *Pfluegers Arch.*, 1913, **150**, 15–45.
89 H. P. Schwan, Electrical properties of tissue and cell suspensions, *Adv. Biol. Med. Phys.*, 1957, **5**, 147–209.
90 H. P. Schwan, Electrode polarization impedance and measurements in biological materials, *Ann. N. Y. Acad. Sci.*, 1968, **148**, 191–209.
91 J. Yang, Y. Huang, X. J. Wang, X. B. Wang, F. F. Becker and P. R. C. Gascoyne, Dielectric properties of human leukocyte subpopulations determined by electrorotation as a cell separation criterion, *Biophys. J.*, 1999, **76**, 3307–3314.
92 X. B. Wang, Y. Huang, P. R. C. Gascoyne, F. F. Becker, R. Holzel and R. Pethig, Changes in Friend Murine Erythroleukemia Cell-Membranes during Induced-Differentiation Determined by Electrorotation, *Biochim. Biophys. Acta, Biomembr.*, 1994, **1193**, 330–344.
93 D. Zimmermann, A. Zhou, M. Kiesel, K. Feldbauer, U. Terpitz, W. Haase, T. Schneider-Hohendorf, E. Bamberg and V. L. Sukhorukov, Effects on capacitance by overexpression of membrane proteins, *Biochem. Biophys. Res. Commun.*, 2008, **369**, 1022–1026.
94 Y. Huang, X. B. Wang, R. Holzel, F. F. Becker and P. R. C. Gascoyne, Electrorotational Studies of the Cytoplasmic Dielectric-Properties of Friend Murine Erythroleukemia-Cells, *Phys. Med. Biol.*, 1995, **40**, 1789–1806.
95 L. Duncan, H. Shelmerdine, M. P. Hughes, H. M. Coley, Y. Hubner and F. H. Labeed, Dielectrophoretic analysis of changes in cytoplasmic ion levels due to ion channel blocker action reveals underlying differences between drug-sensitive and multidrug-resistant leukaemic cells, *Phys. Med. Biol.*, 2008, **53**, N1–N7.
96 R. Holzel, Non-invasive determination of bacterial single cell properties by electrorotation, *Biochim. Biophys. Acta, Mol. Cell Res.*, 1999, **1450**, 53–60.
97 E. Neher and B. Sakmann, Single-Channel Currents Recorded from Membrane of Denervated Frog Muscle-Fibers, *Nature*, 1976, **260**, 799–802.
98 J. H. Nieuwenhuis, F. Kohl, J. Bastemeijer, P. M. Sarro and M. J. Vellekoop, Integrated Coulter counter based on 2-dimensional liquid aperture control, *Sens. Actuators, B*, 2004, **102**, 44–50.
99 J. Zhe, A. Jagtiani, P. Dutta, J. Hu and J. Carletta, A micromachined high throughput Coulter counter for bioparticle detection and counting, *J. Micromech. Microeng.*, 2007, **17**, 304–313.
100 M. W. Shinwari, D. Zhitomirsky, I. A. Deen, P. R. Selvaganapathy, M. J. Deen and D. Landheer, Microfabricated Reference Electrodes and their Biosensing Applications, *Sensors*, 2010, **10**, 1679–1715.
101 J. H. Zhou, K. N. Ren, Y. Z. Zheng, J. Su, Y. H. Zhao, D. Ryan and H. K. Wu, Fabrication of a microfluidic Ag/AgCl reference electrode and its application for portable and disposable electrochemical microchips, *Electrophoresis*, 2010, **31**, 3083–3089.
102 S. Y. Zheng, M. Liu and Y. C. Tai, Micro coulter counters with platinum black electroplated electrodes for human blood cell sensing, *Biomed. Microdevices*, 2008, **10**, 221–231.
103 H. G. Chun, T. D. Chung and H. C. Kim, Cytometry and velocimetry on a microfluidic chip using polyelectrolytic salt bridges, *Anal. Chem.*, 2005, **77**, 2490–2495.
104 K. B. Kim, H. Chun, H. C. Kim and T. D. Chun, Red blood cell quantification microfluidic chip using polyelectrolytic gel electrodes, *Electrophoresis*, 2009, **30**, 1464–1469.
105 H. Choi, K. B. Kim, C. S. Jeon, I. Hwang, S. A. Lee, H. K. Kim, H. C. Kim and T. D. Chung, A label-free DC impedance-based microcytometer for circulating rare cancer cell counting, *Lab Chip*, 2013, **13**, 970–977.
106 R. W. Deblois and C. P. Bean, Counting and Sizing of Submicron Particles by Resistive Pulse Technique, *Rev. Sci. Instrum.*, 1970, **41**, 909.

107 O. A. Saleh and L. L. Sohn, Quantitative sensing of nanoscale colloids using a microchip Coulter counter, *Rev. Sci. Instrum.*, 2001, **72**, 4449–4451.
108 E. G. Cen, C. Dalton, Y. L. Li, S. Adamia, L. M. Pilarski and K. V. I. S. Kaler, A combined dielectrophoresis, traveling wave dielectrophoresis and electrorotation microchip for the manipulation and characterization of human malignant cells, *J. Microbiol. Methods*, 2004, **58**, 387–401.
109 L. Wu, L. Lanry Yung and K. Lim, Dielectrophoretic capture voltage spectrum for measurement of dielectric properties and separation of cancer cells, *Biomicrofluidics*, 2012, **6**, 014113.
110 D. M. Vykoukal, P. R. C. Gascoyne and J. Vykoukal, Dielectric characterization of complete mononuclear and polymorphonuclear blood cell subpopulations for label-free discrimination, *Integr. Biol.*, 2009, **1**, 477–484.
111 L. M. Broche, F. H. Labeed and M. P. Hughes, Extraction of dielectric properties of multiple populations from dielectrophoretic collection spectrum data, *Phys. Med. Biol.*, 2005, **50**, 2267–2274.
112 T. Sun and H. Morgan, Single-cell microfluidic impedance cytometry: a review, *Microfluid. Nanofluid.*, 2010, **8**, 423–443.
113 M. Cristofanilli, G. De Gasperis, L. S. Zhang, M. C. Hung, P. R. C. Gascoyne and G. N. Hortobagyi, Automated electrorotation to reveal dielectric variations related to HER-2/neu overexpression in MCF-7 sublines, *Clin. Cancer Research*, 2002, **8**, 615–619.
114 H. Ying, R. Holzel, R. Pethig and X. B. Wang, Differences in the Ac Electrodynamics of Viable and Nonviable Yeast-Cells Determined through Combined Dielectrophoresis and Electrorotation Studies, *Phys. Med. Biol.*, 1992, **37**, 1499–1517.
115 F. F. Becker, X. B. Wang, Y. Huang, R. Pethig, J. Vykoukal and P. R. C. Gascoyne, Separation of Human Breast-Cancer Cells from Blood by Differential Dielectric Affinity, *Proc. Natl. Acad. Sci. U. S. A.*, 1995, **92**, 860–864.
116 X. B. Wang, Y. Huang, P. R. C. Gascoyne and F. F. Becker, Dielectrophoretic manipulation of particles, *IEEE Trans. Ind. Appl.*, 1997, **33**, 660–669.
117 G. De Gasperis, X. B. Wang, J. Yang, F. F. Becker and P. R. C. Gascoyne, Automated electrorotation: dielectric characterization of living cells by real-time motion estimation, *Meas. Sci. Technol.*, 1998, **9**, 518–529.
118 L. S. Jang and M. H. Wang, Microfluidic device for cell capture and impedance measurement, *Biomed. Microdevices*, 2007, **9**, 737–743.
119 D. Malleo, J. T. Nevill, L. P. Lee and H. Morgan, Continuous differential impedance spectroscopy of single cells, *Microfluid. Nanofluid.*, 2010, **9**, 191–198.
120 K. H. Han, A. Han and A. B. Frazier, Microsystems for isolation and electrophysiological analysis of breast cancer cells from blood, *Biosens. Bioelectron.*, 2006, **21**, 1907–1914.
121 Y. Cho, H. S. Kim, A. B. Frazier, Z. G. Chen, D. M. Shin and A. Han, Whole-Cell Impedance Analysis for Highly and Poorly Metastatic Cancer Cells, *J. Microelectromech. Syst.*, 2009, **18**, 808–817.
122 L.-S. Kung-Chieh Lan, Integration of single-cell trapping and impedance measurement utilizing microwell electrodes, *Biosens. Bioelectron.*, 2010, **26**(5), 2025–2031.
123 S. Li and L. W. Lin, A single cell electrophysiological analysis device with embedded electrode, *Sens. Actuators, A*, 2007, **134**, 20–26.
124 S. B. Cho and H. Thielecke, Micro hole-based cell chip with impedance spectroscopy, *Biosens. Bioelectron.*, 2007, **22**, 1764–1768.
125 C. M. Kurz, H. Büth, A. Sossalla, V. Vermeersch, V. Toncheva, P. Dubruel, E. Schacht and H. Thielecke, Chip-based impedance measurement on single cells for monitoring sub-toxic effects on cell membranes, *Biosens. Bioelectron.*, 2011, **26**, 3405–3412.
126 S. Gawad, L. Schild and P. Renaud, Micromachined impedance spectroscopy flow cytometer for cell analysis and particle sizing, *Lab Chip*, 2001, **1**, 76–82.
127 K. Cheung, S. Gawad and P. Renaud, Impedance spectroscopy flow cytometry: On-chip label-free cell differentiation, *Cytometry, Part A*, 2005, **65A**, 124–132.
128 G. Benazzi, D. Holmes, T. Sun, M. C. Mowlem and H. Morgan, Discrimination and analysis of phytoplankton using a microfluidic cytometer, *IET Nanobiotechnol.*, 2007, **1**, 94–101.
129 D. Holmes, D. Pettigrew, C. H. Reccius, J. D. Gwyer, C. van Berkel, J. Holloway, D. E. Davies and H. Morgan, Leukocyte analysis and differentiation using high speed microfluidic single cell impedance cytometry, *Lab Chip*, 2009, **9**, 2881–2889.
130 K. C. Cheung, M. Di Berardino, G. Schade-Kampmann, M. Hebeisen, A. Pierzchalski, J. Bocsi, A. Mittag and A. Tarnok, Microfluidic Impedance-Based Flow Cytometry, *Cytometry, Part A*, 2010, **77A**, 648–666.
131 X. J. Han, C. van Berkel, J. Gwyer, L. Capretto and H. Morgan, Microfluidic Lysis of Human Blood for Leukocyte Analysis Using Single Cell Impedance Cytometry, *Anal. Chem.*, 2012, **84**, 1070–1075.
132 C. van Berkel, J. D. Gwyer, S. Deane, N. Green, J. Holloway, V. Hollis and H. Morgan, Integrated systems for rapid point of care (PoC) blood cell analysis, *Lab Chip*, 2011, **11**, 1249–1255.
133 G. Mernier, E. Duqi and P. Renaud, Characterization of a novel impedance cytometer design and its integration with lateral focusing by dielectrophoresis, *Lab Chip*, 2012, **12**, 4344–4349.
134 F. B. Myers, C. K. Zarins, O. J. Abilez and L. P. Lee, Label-free electrophysiological cytometry for stem cellderived cardiomyocyte clusters, *Lab Chip*, 2013, **13**, 220–228.
135 J. Riordon, M. Mirzaei and M. Godin, Microfluidic cell volume sensor with tunable sensitivity, *Lab Chip*, 2012, **12**, 3016–3019.
136 C. Kuttel, E. Nascimento, N. Demierre, T. Silva, T. Braschler, P. Renaud and A. G. Oliva, Label-free detection of Babesia bovis infected red blood cells using impedance spectroscopy on a microfabricated flow cytometer, *Acta Trop.*, 2007, **102**, 63–68.
137 G. Schade-Kampmann, A. Huwiler, M. Hebeisen, T. Hessler and M. Di Berardino, On-chip non-invasive and label-free cell discrimination by impedance spectroscopy, *Cell Proliferation*, 2008, **41**, 830–840.
138 C. Bernabini, D. Holmes and H. Morgan, Micro-impedance cytometry for detection and analysis of micron-sized particles and bacteria, *Lab Chip*, 2011, **11**, 407–412.

139 Y. Zheng, E. Shojaei-Baghini, C. Wang and Y. Sun, Microfluidic characterization of specific membrane capacitance and cytoplasm conductivity of single cells, *Biosens. Bioelectron.*, 2012, **42**, 496–502.
140 T. P. Burg, M. Godin, S. M. Knudsen, W. Shen, G. Carlson, J. S. Foster, K. Babcock and S. R. Manalis, Weighing of biomolecules, single cells and single nanoparticles in fluid, *Nature*, 2007, **446**, 1066–1069.
141 M. Godin, F. F. Delgado, S. M. Son, W. H. Grover, A. K. Bryan, A. Tzur, P. Jorgensen, K. Payer, A. D. Grossman, M. W. Kirschner and S. R. Manalis, Using buoyant mass to measure the growth of single cells, *Nat. Methods*, 2010, **7**, 387–U70.
142 M. A. Unger, H. P. Chou, T. Thorsen, A. Scherer and S. R. Quake, Monolithic microfabricated valves and pumps by multilayer soft lithography, *Science*, 2000, **288**, 113–116.
143 Y. C. Kim, J. H. Kang, S. J. Park, E. S. Yoon and J. K. Park, Microfluidic biomechanical device for compressive cell stimulationand lysis, *Sens. Actuators, B*, 2007, **128**, 108–116.
144 Y. C. Kim, S. J. Park and J. K. Park, Biomechanical analysis of cancerous and normal cells based on bulge generation in a microfluidic device, *Analyst*, 2008, **133**, 1432–1439.
145 G. S. Du, A. Ravetto, Q. Fang and J. M. J. den Toonder, Cell types can be distinguished by measuring their viscoelastic recovery times using a micro-fluidic device, *Biomed. Microdevices*, 2011, **13**, 29–40.
146 D. N. Hohne, J. G. Younger and M. J. Solomon, Flexible Microfluidic Device for Mechanical Property Characterization of Soft Viscoelastic Solids Such as Bacterial Biofilms, *Langmuir*, 2009, **25**, 7743–7751.
147 L. A. G. Lin, A. Q. Liu, Y. F. Yu, C. Zhang, C. S. Lim, S. H. Ng, P. H. Yap and H. J. Gao, Cell compressibility studies utilizing noncontact hydrostatic pressure measurements on single living cells in a microchamber, *Appl. Physics Letters*, 2008, **92.**
148 N. Q. Balaban, U. S. Schwarz, D. Riveline, P. Goichberg, G. Tzur, I. Sabanay, D. Mahalu, S. Safran, A. Bershadsky, L. Addadi and B. Geiger, Force and focal adhesion assembly: a close relationship studied using elastic micropatterned substrates, *Nat. Cell Biol.*, 2001, **3**, 466–472.
149 J. L. Tan, J. Tien, D. M. Pirone, D. S. Gray, K. Bhadriraju and C. S. Chen, Cells lying on a bed of microneedles: An approach to isolate mechanical force, *Proc. Natl. Acad. Sci. U. S. A.*, 2003, **100**, 1484–1489.
150 I. Schoen, W. Hu, E. Klotzsch and V. Vogel, Probing Cellular Traction Forces by Micropillar Arrays: Contribution of Substrate Warping to Pillar Deflection, *Nano Lett.*, 2010, **10**, 1823–1830.
151 N. J. Sniadecki, A. Anguelouch, M. T. Yang, C. M. Lamb, Z. Liu, S. B. Kirschner, Y. Liu, D. H. Reich and C. S. Chen, Magnetic microposts as an approach to apply forces to living cells, *Proc. Natl. Acad. Sci. U. S. A.*, 2007, **104**, 14553–14558.
152 R. H. W. Lam, Y. B. Sun, W. Q. Chen and J. P. Fu, Elastomeric microposts integrated into microfluidics for flow-mediated endothelial mechanotransduction analysis, *Lab Chip*, 2012, **12**, 1865–1873.
153 C. Christophis, M. Grunze and A. Rosenhahn, Quantification of the adhesion strength of fibroblast cells on ethylene glycol terminated self-assembled monolayers by a microfluidic shear force assay, *Phys. Chem. Chem. Phys.*, 2010, **12**, 4498–4504.
154 K. V. Christ, K. B. Williamson, K. S. Masters and K. T. Turner, Measurement of single-cell adhesion strength using a microfluidic assay, *Biomed. Microdevices*, 2010, **12**, 443–455.
155 H. Lu, L. Y. Koo, W. C. M. Wang, D. A. Lauffenburger, L. G. Griffith and K. F. Jensen, Microfluidic shear devices for quantitative analysis of cell adhesion, *Anal. Chem.*, 2004, **76**, 5257–5264.
156 S. Usami, H. H. Chen, Y. H. Zhao, S. Chien and R. Skalak, Design and Construction of a Linear Shear-Stress Flow Chamber, *Ann. Biomed. Eng.*, 1993, **21**, 77–83.
157 E. Gutierrez and A. Groisman, Quantitative measurements of the strength of adhesion of human neutrophils to a substratum in a microfluidic device, *Anal. Chem.*, 2007, **79**, 2249–2258.
158 P. Rupprecht, L. Gole, J. P. Rieu, C. Vezy, R. Ferrigno, H. C. Mertani and C. Riviere, A tapered channel microfluidic device for comprehensive cell adhesion analysis, using measurements of detachment kinetics and shear stress-dependent motion, *Biomicrofluidics*, 2012, **6.**
159 K. Goda, A. Ayazi, D. R. Gossett, J. Sadasivam, C. K. Lonappan, E. Sollier, A. M. Fard, S. C. Hur, J. Adam, C. Murray, C. Wang, N. Brackbill, D. Di Carlo and B. Jalali, High-throughput single-microparticle imaging flow analyzer, *Proc. Natl. Acad. Sci. U. S. A.*, 2012, **109**, 11630–11635.
160 D. Barat, D. Spencer, G. Benazzi, M. C. Mowlem and H. Morgan, Simultaneous high speed optical and impedance analysis of single particles with a microfluidic cytometer, *Lab Chip*, 2012, **12**, 118–126.
161 D. Holmes and H. Morgan, Single Cell Impedance Cytometry for Identification and Counting of CD4 T-Cells in Human Blood Using Impedance Labels, *Anal. Chem.*, 2010, **82**, 1455–1461.